A&A 587, A39 (2016)
DOI: 10.1051/0004-6361/201527324

Astronomy & Astrophysics

Stellar laboratories

VI. New Mo IV–VII oscillator strengths and the molybdenum abundance in the hot white dwarfs G191−B2B and RE 0503−289⋆,⋆⋆,⋆⋆⋆

T. Rauch[1], P. Quinet[2,3], D. Hoyer[1], K. Werner[1], M. Demleitner[4], and J. W. Kruk[5]

[1] Institute for Astronomy and Astrophysics, Kepler Center for Astro and Particle Physics, Eberhard Karls University, Sand 1, 72076 Tübingen, Germany
e-mail: rauch@astro.uni-tuebingen.de
[2] Physique Atomique et Astrophysique, Université de Mons – UMONS, 7000 Mons, Belgium
[3] IPNAS, Université de Liège, Sart Tilman, 4000 Liège, Belgium
[4] Astronomisches Rechen-Institut, Zentrum für Astronomie, Ruprecht Karls University, Mönchhofstraße 12-14, 69120 Heidelberg, Germany
[5] NASA Goddard Space Flight Center, Greenbelt, MD 20771, USA

Received 8 September 2015 / Accepted 13 December 2015

ABSTRACT

Context. For the spectral analysis of high-resolution and high signal-to-noise (S/N) spectra of hot stars, state-of-the-art non-local thermodynamic equilibrium (NLTE) model atmospheres are mandatory. These are strongly dependent on the reliability of the atomic data that is used for their calculation.
Aims. To identify molybdenum lines in the ultraviolet (UV) spectra of the DA-type white dwarf G191−B2B and the DO-type white dwarf RE 0503−289 and, to determine their photospheric Mo abundances, reliable Mo IV–VII oscillator strengths are used.
Methods. We newly calculated Mo IV–VII oscillator strengths to consider their radiative and collisional bound-bound transitions in detail in our NLTE stellar-atmosphere models for the analysis of Mo lines exhibited in high-resolution and high S/N UV observations of RE 0503−289.
Results. We identified 12 Mo V and 9 Mo VI lines in the UV spectrum of RE 0503−289 and measured a photospheric Mo abundance of $1.2-3.0 \times 10^{-4}$ (mass fraction, 22 500−56 400 times the solar abundance). In addition, from the As V and Sn IV resonance lines, we measured mass fractions of arsenic ($0.5-1.3 \times 10^{-5}$, about 300−1200 times solar) and tin ($1.3-3.2 \times 10^{-4}$, about 14 300−35 200 times solar). For G191−B2B, upper limits were determined for the abundances of Mo (5.3×10^{-7}, 100 times solar) and, in addition, for Kr (1.1×10^{-6}, 10 times solar) and Xe (1.7×10^{-7}, 10 times solar). The arsenic abundance was determined ($2.3-5.9 \times 10^{-7}$, about 21−53 times solar). A new, registered German Astrophysical Virtual Observatory (GAVO) service, TOSS, has been constructed to provide weighted oscillator strengths and transition probabilities.
Conclusions. Reliable measurements and calculations of atomic data are a prerequisite for stellar-atmosphere modeling. Observed Mo V-VI line profiles in the UV spectrum of the white dwarf RE 0503−289 were well reproduced with our newly calculated oscillator strengths. For the first time, this allowed the photospheric Mo abundance in a white dwarf to be determined.

Key words. atomic data – line: identification – stars: abundances – stars: individual: G191-B2B – stars: individual: RE0503-289 – virtual observatory tools

1. Introduction

RE 0503−289 (WD 0501−289, McCook & Sion 1999a,b) is a hot, helium-rich, DO-type white dwarf (WD, effective temperature $T_{\rm eff}$ = 70 000 K, surface gravity $\log(g/{\rm cm/s^2}) = 7.5$, Dreizler & Werner 1996), that exhibits lines of at least ten trans-iron elements in its far-ultraviolet (FUV) spectrum (Werner et al. 2012b). The abundance analysis of these species is hampered by the lack of atomic data for their higher ionization stages, i.e., IV-VII. While Werner et al. (2012b) could measure only the Kr and Xe abundances, further abundance determinations (Zn, Ge, Ga, Xe, and Ba by Rauch et al. 2014a, 2012, 2014b, 2015b,a, respectively) were always initiated by new calculations of reliable transition probabilities.

G191−B2B (WD 0501+527, McCook & Sion 1999a,b) is a hot, hydrogen-rich, DA-type white dwarf that was recently analyzed by Rauch et al. (2013, $T_{\rm eff}$ = 60 000 K, $\log g = 7.6$). Based on this model, Rauch et al. (2014a,b, 2015b) measured the abundances of Zn, Ba, and Ga.

Molybdenum is another trans-iron element (atomic number Z = 42). It was discovered for the first time in a WD (in the spectrum of RE 0503−289) by Werner et al. (2012b, four Mo VI lines). To identify more lines of Mo and to determine its abundance, we calculated new transition probabilities for Mo IV–VII.

In this paper, we first describe the available observations (Sect. 2), our stellar-atmosphere models (Sect. 3), and the

⋆ Based on observations with the NASA/ESA *Hubble* Space Telescope, obtained at the Space Telescope Science Institute, which is operated by the Association of Universities for Research in Astronomy, Inc., under NASA contract NAS5-26666.
⋆⋆ Based on observations made with the NASA-CNES-CSA Far Ultraviolet Spectroscopic Explorer.
⋆⋆⋆ Tables A.10–A.13 are only available via the German Astrophysical Virtual Observatory (GAVO) service TOSS (http://dc.g-vo.org/TOSS).

computation of the new transition probabilities (Sect. 4). A new Virtual Observatory (VO) service that provides access to transition probabilities is presented in Sect. 5.

To use the most elaborated models of G191−B2B and RE 0503−289 for our Mo abundance analysis, we start with an incorporation and an abundance determination of arsenic (Sect. 6.1, both stars) and tin (Sect. 6.2, RE 0503−289). Then, we assess the Mo photospheric abundances in RE 0503−289 and G191−B2B (Sect. 6.3). In Sect. 6.5, we determine upper abundance limits of krypton and xenon in G191−B2B. To understand the abundance patterns of trans-iron elements, we investigate on the efficiency of radiative levitation acting on the elements Zn, Ga, Ge, As, Kr, Mo, Sn, Xe, and Ba in both stars' atmospheres (Sect. 7). We summarize our results and conclude in Sect. 8.

2. Observations

G191−B2B. We used the spectra obtained with the Far Ultraviolet Spectroscopic Explorer (FUSE, 910 Å $< \lambda <$ 1190 Å, resolving power $R = \lambda/\Delta\lambda \approx 20\,000$, for details see Rauch et al. 2013) and the *Hubble* Space Telescope/Space Telescope Imaging Spectrograph (HST/STIS, 1145 Å $< \lambda <$ 3145 Å, resolution of ≈3 km s^{-1}, see Rauch et al. 2013[1]).

RE 0503−289. We analyzed its FUSE (described in detail by Werner et al. 2012b) and HST/STIS observations (1144 Å $< \lambda <$ 3073 Å). The latter was co-added from two observations with grating E140M (exposure times 2493 s and 3001 s, 1144−1709 Å, $R \approx 45\,800$), and two observations with grating E230M (1338 s, 1690−2366 Å and 1338 s, 2277−3073 Å, $R \approx 30\,000$). These STIS observations are retrievable from the Barbara A. Mikulski Archive for Space Telescopes (MAST).

3. Model atmospheres and atomic data

We employed the Tübingen NLTE[2] Model Atmosphere Package (TMAP[3], Werner et al. 2003, 2012a) to calculate plane-parallel, chemically homogeneous model-atmospheres in hydrostatic and radiative equilibrium. Model atoms were taken from the Tübingen Model Atom Database (TMAD[4], Rauch & Deetjen 2003) that has been constructed as part of the Tübingen contribution to the German Astrophysical Virtual Observatory (GAVO[5]). For our Mo model atoms, we follow Rauch et al. (2015b) and used a statistical approach to calculate so-called super levels and super lines with our Iron Opacity and Interface (IrOnIc[6], Rauch & Deetjen 2003). We transferred our new Mo data into Kurucz-formatted files[7] that were then ingested and processed by IrOnIc. The statistics of our Mo model atom is summarized in Table 1.

For Mo and all other species, level dissolution (pressure ionization) following Hummer & Mihalas (1988) and Hubeny et al. (1994) is accounted for. Broadening for all Mo lines that are due to the quadratic Stark effect is calculated using approximate formulae by Cowley (1970, 1971).

Table 1. Statistics of Mo IV - VII atomic levels and line transitions from Tables A.10–A.13, respectively.

Ion	Atomic levels	Lines	Super levels	Super lines
IV	162	2803	7	15
V	257	5882	7	22
VI	112	988	7	23
VII	95	1181	7	16
	626	10 824	28	76

4. Atomic structure and radiative data calculation

New calculations of oscillator strengths for a large number of transitions of molybdenum ions that are considered in the present work were carried out using the pseudo-relativistic Hartree-Fock (HFR) method (Cowan 1981), including core-polarization corrections (see, e.g., Quinet et al. 1999, 2002).

For Mo IV, the configuration interaction was considered among the configurations $4d^3$, $4d^2 5s$, $4d^2 6s$, $4d^2 5d$, $4d^2 6d$, $4d4f^2$, $4d5s^2$, $4d5p^2$, $4d5d^2$, 4d5s5d, 4d5p4f, 4d5p5f, and 4d4f5f for the even parity and $4d^2 5p$, $4d^2 6p$, $4d^2 4f$, $4d^2 5f$, 4d5s5p, 4d5s4f, 4d5s5f, 4d5p5d, 4d4f5d, and 4d5d5f for the odd parity. The core-polarization parameters were the dipole polarizability of a Mo VII ionic core reported by Fraga et al. (1976), i.e., $\alpha_d = 1.82$ au, and the cut-off radius corresponding to the HFR mean value $\langle r \rangle$ of the outermost core orbital (4p), i.e., $r_c = 1.20$ au. Using the experimental energy levels reported by Sugar & Musgrove (1988) and Cabeza et al. (1989), the radial integrals (average energy, Slater, spin-orbit and effective interaction parameters) of $4d^3$, $4d^2 5s$, $4d^2 6s$, $4d^2 5d$, and $4d^2 5p$ configurations were adjusted by a well-established least-squares fitting process that minimizes the differences between computed and experimental energies.

For Mo V, the configurations retained in the HFR model were $4d^2$, 4d5s, 4d6s, 4d5d, 4d6d, 4d5g, $5s^2$, $5p^2$, $5d^2$, $4f^2$, 5s5d, 5s6s, 5p4f, 5p5f, $4p^5 4d^2 4f$, $4p^5 4d^2 5f$, and $4p^5 4d^2 5p$ for the even parity and 4d5p, 4d6p, 4d4f, 4d5f, 4d6f, 4d7f, 4d8f, 4d9f, 5s5p, 5p5d, 5s4f, 5s5f, 4f5d, $4p^5 4d^3$, $4p^5 4d^2 5s$, and $4p^5 4d^2 5d$ for the odd parity. In this ion, the semi-empirical process was performed to optimize the radial integrals corresponding to $4d^2$, 4d5s, 4d6s, 4d5d, 4d5g, $5s^2$, $5p^2$, 5s5d, 5s6s, 4d5p, 4d6p, 4d4f, 4d5f, 4d6f, 4d7f, 4d8f, 4d9f, 5s5p, 5s4f, and $4p^5 4d^3$ configurations, which use the experimental energy levels reported by Reader & Tauheed (2015). Core-polarization effects were estimated using a dipole polarizability value corresponding to a Mo VIII ionic core taken from Fraga et al. (1976), i.e., $\alpha_d = 1.48$ au, and a cut-off radius equal to 1.20 au.

In the case of Mo VI, the 4d, 5d, 6d, 7d, 8d, 5s, 6s, 7s, 8s, 5g, 6g, 7g, 8g, 7i, 8i, $4p^5 4d5p$, $4p^5 4d4f$, and $4p^5 4d5f$ even configurations and the 5p, 6p, 7p, 8p, 9p, 10p, 11p, 4f, 5f, 6f, 7f, 8f, 9f, 6h, 7h, 8h, 8k, $4p^5 4d^2$, $4p^5 4d5s$, and $4p^5 4d5d$ odd configurations were explicitly included in the HFR model with the same core-polarization parameters as those considered for Mo V. The semi-empirical optimization process was carried out to fit the radial parameters in the nd ($n = 4$−8), ns ($n = 5$−8), ng ($n = 5$−8), ni ($n = 7$−8), np ($n = 5$−11), nf ($n = 4$−9), nh ($n = 6$−8), 8k, $4p^5 4d^2$, and $4p^5 4d5s$ configurations using the experimental energy levels published by Reader (2010).

[1] Available at http://www.stsci.edu/hst/observatory/cdbs/calspec.html
[2] Non-local thermodynamic equilibrium.
[3] http://astro.uni-tuebingen.de/~TMAP
[4] http://astro.uni-tuebingen.de/~TMAD
[5] http://www.g-vo.org
[6] http://astro.uni-tuebingen.de/~TIRO
[7] GFxxyy.GAM, GFxxyy.LIN, and GFxxyy.POS files with xx = element number, yy = element charge, http://kurucz.harvard.edu/atoms.html

Finally, for Mo VII, the HFR multiconfiguration expansions included the $4p^6$, $4p^55p$, $4p^56p$, $4p^54f$, $4p^55f$, $4p^56f$, $4s4p^64d$, $4s4p^65d$, $4s4p^66d$, $4s4p^65s$, $4s4p^66s$, $4p^44d^2$, $4p^44d5s$, and $4p^45s^2$ even configurations and the $4p^54d$, $4p^55d$, $4p^56d$, $4p^55s$, $4p^56s$, $4p^57s$, $4p^58s$, $4p^59s$, $4p^510s$, $4p^55g$, $4p^56g$, $4s4p^65p$, $4s4p^66p$, $4s4p^64f$, $4s4p^65f$, $4s4p^66f$, $4p^44d5p$, and $4p^44d4f$ odd configurations. Here, because some configurations with open 4s and 4p orbitals were explicitly included in the physical model, the core-polarization effects were estimated by considering a Mo XV ionic core with the corresponding dipole polarizability value taken from Johnson et al. (1983), i.e., $\alpha_d = 0.058$ au, and a cut-off radius equal to 0.41 a.u, which corresponds to the HFR mean value $\langle r \rangle$ of the 3d subshell. The fitting process was then carried out with the experimental energy levels classified by Sugar & Musgrove (1988) and Shirai et al. (2000) to adjust the radial parameters that characterize the $4p^6$, $4p^55p$, $4p^54f$, $4p^55f$, $4s4p^64d$, $4p^44d^2$, $4p^54d$, $4p^55d$, $4p^5ns$ ($n = 5-10$), $4p^55g$, and $4s4p^65p$ configurations. The parameters adopted in our computations are summarized in Tables A.1–A.4 and computed and available experimental energies are compared in Tables A.5–A.8, for Mo IV–VII, respectively.

Tables A.10–A.13 give the weighted HFR oscillator strengths ($\log gf$) and transition probabilities (gA, in s^{-1}) for Mo IV–VII, respectively, and the numerical values (in cm^{-1}) of lower and upper energy levels and the corresponding wavelengths (in Å). In the last column of each table, we also give the absolute value of the cancellation factor CF, as defined by Cowan (1981). We note that very low values of this factor (typically <0.05) indicate strong cancellation effects in the calculation of line strengths. In these cases, the corresponding gf and gA values could be very inaccurate and, therefore, need to be considered with some care. However, very few of the transitions that appear in Tables A.10–A.13 are affected. These tables are provided via the newly developed GAVO Tübingen Oscillator Strengths Service TOSS[8] that is briefly described in Sect. 5.

Oscillator strengths were published by Reader & Tauheed (2015) for 923 lines of Mo V and by Reader (2010) for 245 lines of Mo VI. We compared $\log gf$ values and wavelengths of those lines whose positions agree with those of our lines within $\Delta\lambda \leq 0.02$ Å (these are 921 lines of Mo V, 178 lines of Mo VI) (Figs. 1 and 2). In general, we find a rather good agreement, although our new $\log gf$-values seem to be, on average, smaller than those previously published. This can be explained by the fact that our calculations explicitly include a larger set of interacting configurations, in particular with an open 4p subshell, as well as a pseudo-potential modeling of the remaining core-valence electronic correlations. For the Mo V and Mo VI lines that were identified in RE 0503−289 (Table A.9, Fig. 12) and were used for the abundance determination, the $\log gf$-values are almost identical.

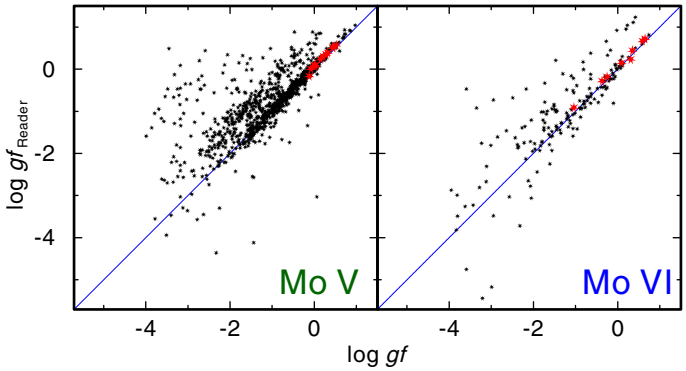

Fig. 1. Comparison of our weighted oscillator strengths to those of Reader & Tauheed (2015) for Mo V (*left*) and of Reader (2010) for Mo VI (*right*). The larger, red symbols refer to the lines identified in RE 0503−289 (Table A.9).

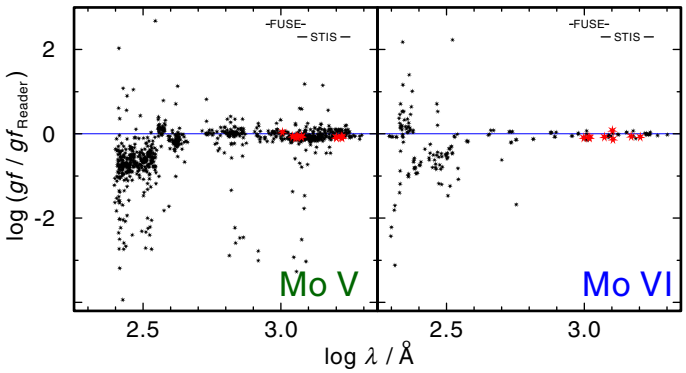

Fig. 2. Ratio of our weighted oscillator strengths and those of Reader & Tauheed (2015) for Mo V (*left*) and of Reader (2010) for Mo VI (*right*). The wavelength ranges of our FUSE and HST/STIS spectra are marked. The larger, red symbols refer to the lines identified in RE 0503−289 (Table A.9).

5. The GAVO service TOSS

In the framework of the GAVO project, we developed the new, registered VO service TOSS. It is designed to provide easy access to calculated oscillator strengths and transition probabilities of any kind in VO-compliant format.

Line data is stored in terms of the Spectral Line Data Model (Osuna et al. 2010) and is accessible through a web browser interface, via the Simple Line Access Protocol SLAP (Salgado et al. 2010), and via the Table Access Protocol TAP (Dowler et al. 2010). The browser-based interface offers a web form, which allows conventional queries by wavelength, element, ionisation stage, etc., exporting to various tabular formats and also directly into user programs via SAMP[9].

The SLAP interface can be used from specialized programs ("SLAP clients") like VOSpec (Osuna et al. 2005); this is normally transparent to the user; in a server selector, the service will typically appear under its short name TOSS SLAP.

The TAP interface allows database queries against the line database, including comparisons with user-provided data ("uploads"). In the TAP dialogs of applications like TOPCAT, the user should look for "GAVO DC" or manually enter the access URL[10]. As the discussion of TAP's possibilities is beyond the scope of this paper, see on-line examples for TOSS service usage[11].

6. Photospheric abundances

To improve the simulation of the background opacity, we included As in our calculations for G191−B2B and RE 0503−289 and determined its abundance from these models (Sect. 6.1). Then, we included Sn for RE 0503−289 (Sect. 6.2) because our

[8] http://dc.g-vo.org/TOSS

[9] The Simple Application Messaging Protocol is a VO-defined standard protocol facilitating seamless and fast data exchange on user desktops.

[10] http://dc.g-vo.org/tap

[11] http://dc.g-vo.org/toss/q/q/examples

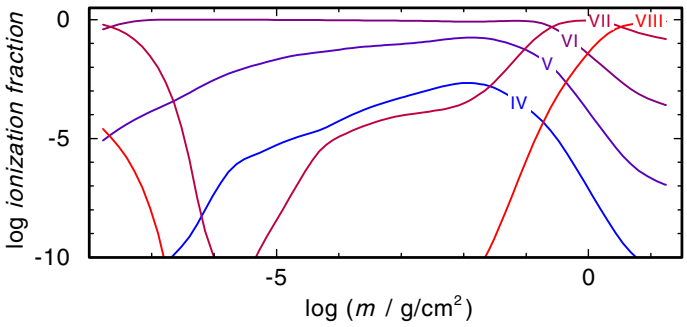

Fig. 3. Arsenic ionization fractions in our RE 0503−289 model. m is the column mass, measured from the outer boundary of the model atmosphere.

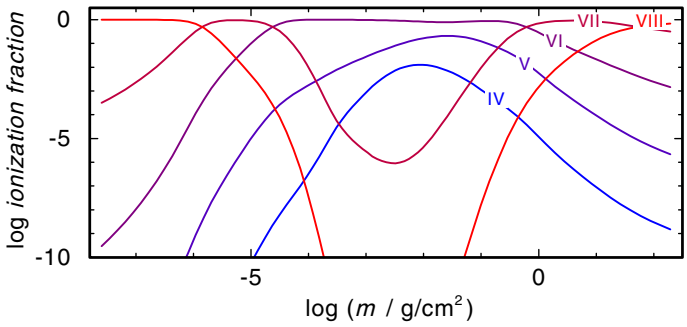

Fig. 4. As in Fig. 3, for G191−B2B.

new HST/STIS observation provides access to Sn IV lines that are necessary for an abundance analysis. Based on these extended models, we considered Mo and determined its abundances for RE 0503−289 (Sect. 6.3) and G191−B2B (Sect. 6.4).

6.1. G191-B2B and RE 0503-289: Arsenic (Z = 33)

In the FUSE observation of RE 0503−289, Werner et al. (2012b) discovered As V $\lambda\lambda$ 987.65, 1029.48, 1051.6, 1056.7 Å. For As V, lifetimes were measured with the beam-foil technique (Pinnington et al. 1981). The multiplet f-value (0.78 ± 0.06) of the As V resonance transition was determined with the help of arbitrarily normalized decay curve (ANDC) analyses, which were confirmed by calculations of Fischer (1977), Migdalek & Baylis (1979), and Curtis & Theodosiou (1989). Morton (2000) lists both components in his compilation, λ 987.65 Å ($4s\,^2S_{1/2}$−$4p\,^2P^\circ_{3/2}$, f = 0.528) and λ 1029.48 Å ($4s\,^2S_{1/2}$−$4p\,^2P^\circ_{1/2}$, f = 0.253). These were used by Chayer et al. (2015) to determine arsenic mass fractions. They found 6.3×10^{-8} (6 times solar) and 1.6×10^{-5} (1450 times solar) in G191−B2B and RE 0503−289, respectively.

As V $\lambda\lambda$ 1051.6, 1056.7 Å belong to the $4d\,^2D$−$4f\,^2F^\circ$ multiplet ($\lambda\lambda$1050.67, 1051.64, 1055.60, 1056.58) but no oscillator strengths have been calculated so far.

We included the TMAD As IV-VIII model atom in our model-atmosphere calculations. As VI is the dominant ion in the line-forming region in both stars (Figs. 3 and 4). We reproduced the observed As V $\lambda\lambda$ 987.65, 1029.48 Å line profiles well in the FUSE spectra of G191−B2B and RE 0503−289 at mass fractions of 3.7×10^{-7} (29 times solar) and 8.3×10^{-6} (760 times solar), respectively (Fig. 5). Our abundances deviate by factors of 6 and 0.5 for G191−B2B and RE 0503−289, respectively, from those of Chayer et al. (2015), who made an LTE assumption because of lack of atomic data. Both stars are out of the validity domain for LTE modeling (e.g., Rauch 2012), which is corroborated by an inspection of the departure coefficients (ratio of NLTE to LTE occupation numbers) of the five lowest As V levels in our models for G191−B2B and RE 0503−289 that deviate from unity (Fig. 6 and 7, respectively). Therefore, the results of an LTE analysis may be afflicted by a large systematic error.

Figure 8 shows a comparison of theoretical profiles of As V $\lambda\lambda$ 987.65, 1029.48 Å that are calculated from our NLTE model and an LTE model (calculated by TMAD based on the temperature and density stratification of the NLTE model, LTE occupation numbers of the atomic levels are enforced by an artificial increase of all collisional rates by a factor of 10^{20}). In the case of G191−B2B, the LTE profiles are too strong and, thus,

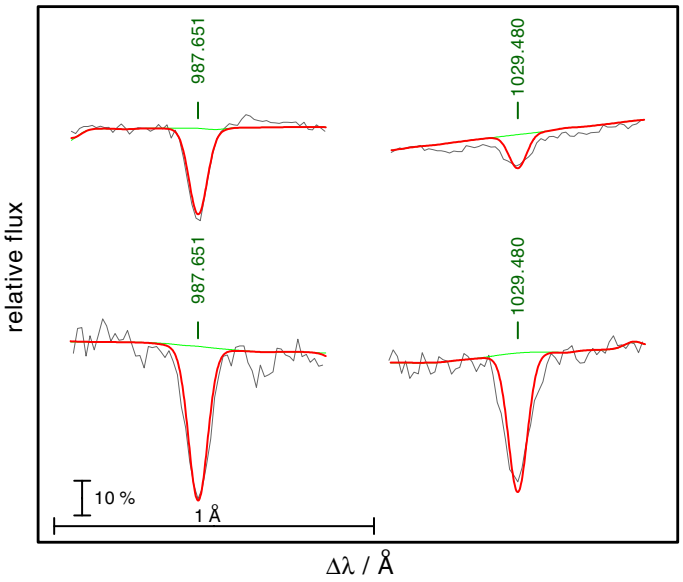

Fig. 5. Sections of our FUSE observations of G191−B2B (*top row*) and RE 0503−289 (*bottom row*) around As V λ 987.65 Å (*left column*) and As V λ 1029.48 Å (*right column*). The thick red and thin green lines show a comparison with theoretical spectra of two models, with and without As, respectively.

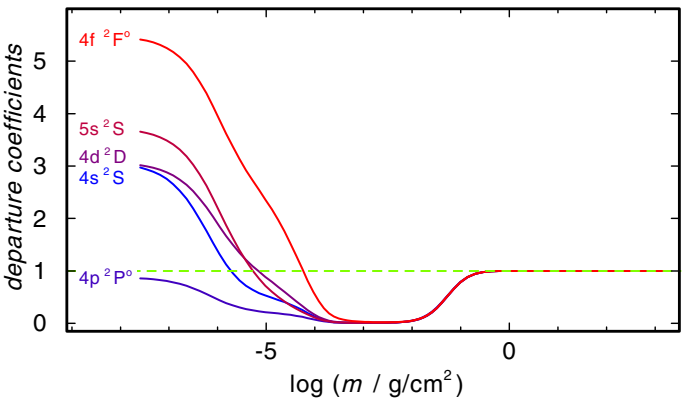

Fig. 6. Departure coefficients of the five lowest As V levels in the model for G191−B2B.

the abundance had to be reduced to 1.0×10^{-7} to match the observation. For RE 0503−289, they are too weak and, thus, a higher abundance of 1.7×10^{-5} is needed to reproduce the observation. This may explain, in part, the deviation of our As abundances from those of Chayer et al. (2015).

However, a precise abundance analysis by means of NLTE model-atmosphere techniques requires reliable oscillator

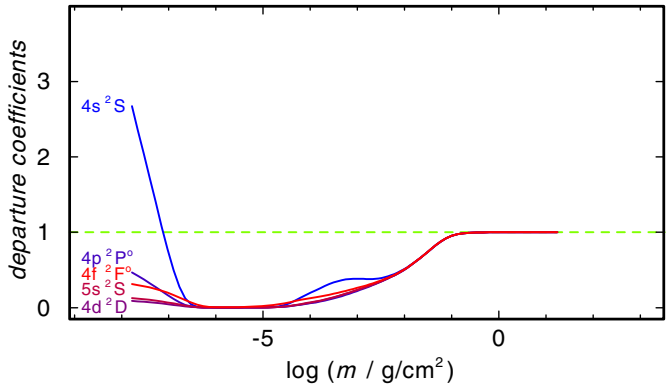

Fig. 7. As for Fig. 6, for RE 0503−289.

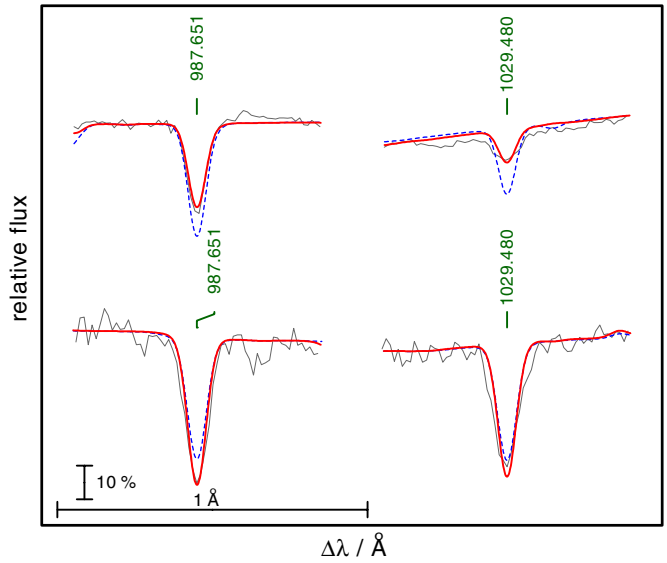

Fig. 8. As for Fig. 5, the thick red and dashed blue lines show a comparison with theoretical spectra of NLTE and LTE models, respectively.

strengths, not only for the lines employed in the abundance determination, but for the complete model atom that is considered in the model-atmosphere and spectral-energy-distribution calculations. Once these oscillator strengths become available for a large number of As V-VII lines, it will be possible to construct much more complete As model ions and a new determination of the As abundance will be more precise.

6.2. RE 0503-289: Tin (Z = 50)

Rauch et al. (2013) measured the Sn abundance in G191−B2B (3.53×10^{-7}, 37 times solar). They used the lines of the resonance doublet, namely, Sn IV λ 1314.537 Å ($5s\,^2S_{1/2}$−$5p\,^2P^\circ_{3/2}$, $f = 0.637$) and λ 1437.525 Å ($5s\,^2S_{1/2}$−$5p\,^2P^\circ_{1/2}$, $f = 0.240$). Their f-values were calculated by Morton (2000) based on energy levels provided by Moore (1958). These lines are visible in our HST/STIS spectrum of RE 0503−289 as well. To determine the Sn abundance, we used the same model atom like Rauch et al. (2013) and reproduced the observed line profiles of both lines (Fig. 9) well at a mass fraction of 2.04×10^{-4} (about 22 500 times solar). This Sn abundance analysis will also be improved, as soon as reliable transition probabilities for Sn IV-VI are published.

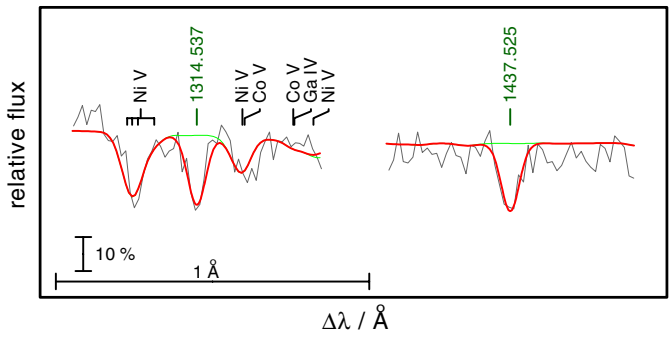

Fig. 9. Sections of our HST/STIS observations of RE 0503−289 around Sn IV λ 1314.537 Å (*left*) and Sn IV λ 1427.525 Å (*right*). The thick, red and thin, green lines show a comparison with theoretical spectra of two models with and without Sn, respectively.

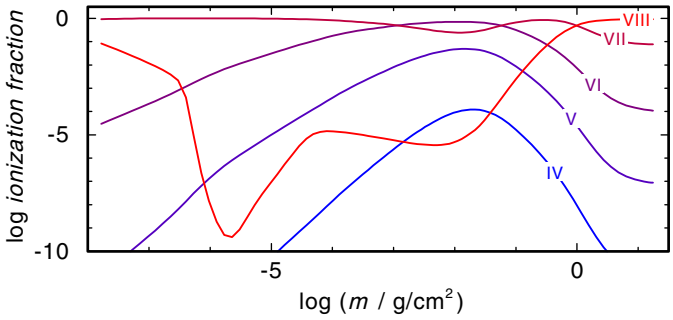

Fig. 10. Molybdenum ionization fractions in our RE 0503−289 model.

6.3. RE 0503-289: Molybdenum

Our RE 0503−289 model ($T_{\rm eff}$ = 70 000 K, log g = 7.5) includes opacities of H, He, C, N, O, Si, P, S, Ca, Sc, Ti, V, Cr, Mn, Fe, Co, Ni, Zn, Ga, Ge, As, Kr, Mo, Xe, and Ba. Figure 10 shows the Mo ionization fractions in this model. Mo VI+VII are the dominating ionization stages in the line-forming region ($-4.0 \lesssim \log m \lesssim 0.5$). The element abundances are given in Table 2. In general, their uncertainty is about 0.2 dex. This includes the error propagation due to the error ranges of $T_{\rm eff}$ (cf., e.g., Vennes & Lanz 2001), log g, and the background opacity.

Figure 11 shows the relative line strengths (normalized to that of Mo VI λ 1038.642 Å) of the Mo lines in the synthetic spectrum of RE 0503−289. We note that these strengths reduce if the spectrum is convolved with a Gaussian to match the instruments' resolutions (Sect. 2).

In the FUSE and HST/STIS observations, we identified 12 Mo V and nine Mo VI lines (Fig. 12). Their strengths were well reproduced at a Mo abundance of 1.88×10^{-4} (mass fraction), which is 35 400 times the solar value (Grevesse et al. 2015). Many more weak Mo V and Mo VI lines are visible in the synthetic spectrum but they fade in the noise of the presently available observations. The search for the strongest Mo IV and Mo VII lines (Fig. 11) was not successful. This was not unexpected, given the predicted weakness of the lines and the S/N of the data. Figure 13 shows the two strongest Mo VII lines of our model. We note that Ba VII λ 1255.520 Å dominates the observed absorption around λ1255.5 Å (Fig. 13).

The identification of Mo lines in the wavelength region $\lambda \gtrsim 1700$ Å was strongly hampered by the lower signal-to-noise (S/N) and resolution (only a fourth of the exposure time and 66% of the resolving power of the spectrum, compared to the region at $\lambda \lesssim 1700$ Å, see Sect. 2). An example is shown in

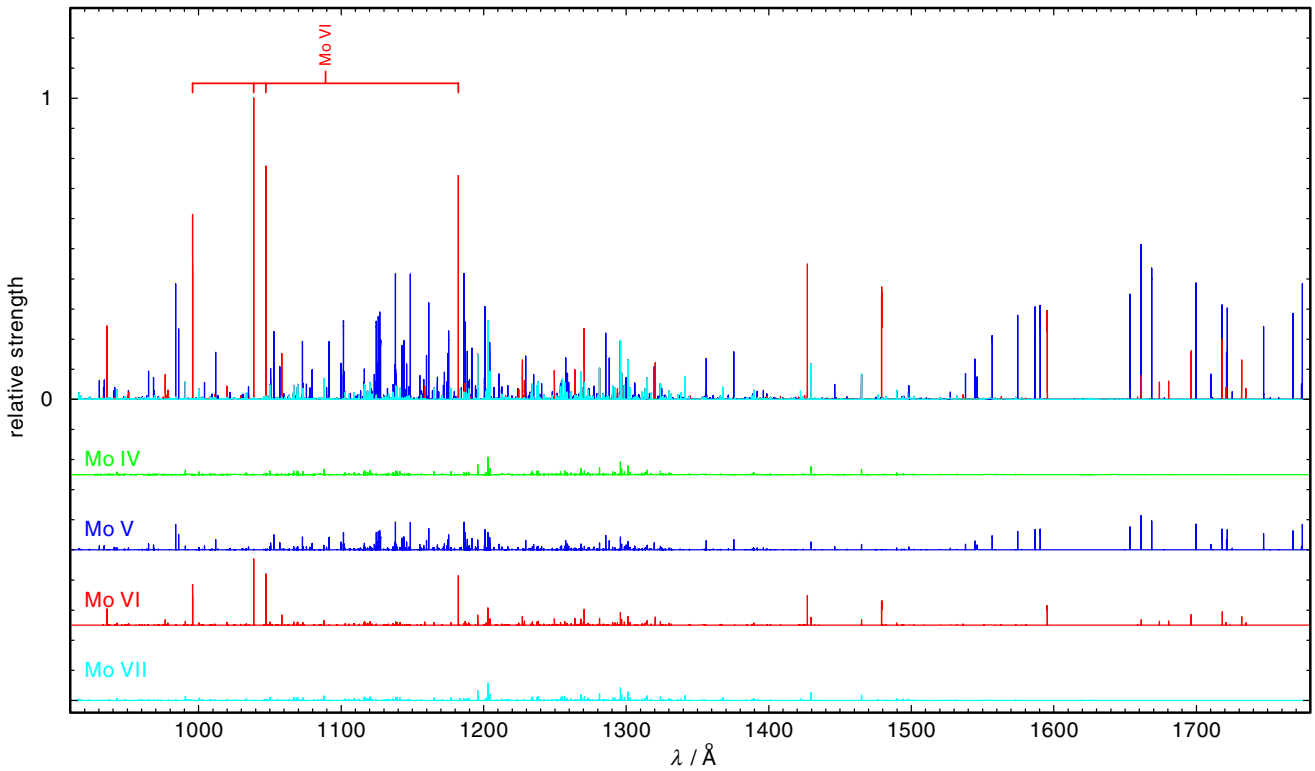

Fig. 11. Relative strengths of Mo lines calculated from our stellar-atmosphere model of RE 0503−289. Top graph: Mo IV–VII lines, the four most prominent are Mo VI lines that were identified by Werner et al. (2012b) are marked. Graphs 2 to 5 (from top to bottom): lines of individual Mo IV–VII ions (intensities reduced by a factor of 0.22 compared to the top graph), respectively.

Table 2. Photospheric abundances of RE 0503−289.

Element	Mass Fraction	Number Fraction	[X]
He	9.74×10^{-1}	9.92×10^{-1}	0.592
C	2.23×10^{-2}	7.56×10^{-3}	0.974
N	1.73×10^{-4}	5.04×10^{-5}	−0.602
O	1.97×10^{-3}	5.01×10^{-4}	−0.464
Si	1.61×10^{-4}	2.33×10^{-5}	−0.617
P	1.15×10^{-6}	1.51×10^{-7}	−0.705
S	3.96×10^{-5}	5.04×10^{-6}	−0.892
IG	1.00×10^{-6}	9.19×10^{-8}	−1.787
Fe	$<1.30 \times 10^{-5}$	$<9.50 \times 10^{-7}$	<−1.967
Ni	7.26×10^{-5}	5.04×10^{-6}	0.028
Zn	1.13×10^{-4}	7.05×10^{-6}	1.814
Ga	3.45×10^{-5}	2.02×10^{-6}	2.810
Ge	1.59×10^{-4}	8.90×10^{-6}	2.845
As	8.27×10^{-6}	4.50×10^{-7}	2.879
Kr	5.05×10^{-5}	2.46×10^{-6}	2.666
Mo	1.88×10^{-4}	8.00×10^{-6}	4.549
Sn	2.04×10^{-4}	7.00×10^{-6}	4.351
Xe	6.30×10^{-5}	1.96×10^{-6}	3.577
Ba	3.58×10^{-4}	1.06×10^{-5}	4.301

Notes. IG is a generic model atom (Rauch & Deetjen 2003) comprising Ca, Sc, Ti, V, Cr, Mn, and Co. [X] denotes log (fraction/solar fraction) of species X.

Fig. 14. Mo V λ 1718.088 Å appears at comparable strengths of other lines that were identified (Fig. 12). However, it is within the noise level of the observation and has to be judged uncertain. Mo VI λ 1718.238 Å is weaker but a better observation would allow an identification.

6.4. G191-B2B: Molybdenum

We added Mo into our atmosphere model ($T_{\rm eff}$ = 60 000 K, $\log g = 7.6$) for G191−B2B, which considers H, He, C, N, O, Al, Si, P, S, Ca, Sc, Ti, V, Cr, Mn, Fe, Co, Ni, Zn, Ga, Ge, As, Mo, Sn, and Ba. The abundances are given in Table 3. Mo VI+VII are the dominating ionization fractions in the line-forming region (Fig. 15).

We performed a search for Mo lines in the observed spectra of G191−B2B, analogous to that in Sect. 6.3. However, we did not identify any. Figure 16 shows a comparison of our synthetic spectra to the observations. Since the HST/STIS spectrum of G191−B2B (Sect. 2) is of excellent quality, Mo VI λ 1469.168 Å gives a stringent upper abundance limit of 5.3×10^{-7} by mass (about 100 times solar, Grevesse et al. 2015).

6.5. G191-B2B: Krypton (Z = 36) and Xenon (Z = 54)

For G191−B2B, we have determined a relatively high upper abundance limit (about 100 times solar) for Mo (Sect. 6.4). This is well in agreement with a factor of about 100−1000 between the trans-iron element abundances in RE 0503−289 and G191−B2B. Like Mo, Kr, and Xe exhibit prominent lines in the UV spectra of RE 0503−289, but not in those of G191−B2B. To investigate on their abundances, we individually included Kr and Xe in our G191−B2B models and calculated theoretical profiles for all Kr and Xe lines that were identified in RE 0503−289 (Werner et al. 2012b; Rauch et al. 2015a). An upper Kr abundance limit of 10 times solar (1.09×10^{-6} by mass) is determined from lines of Kr VI-VII simultaneously (Fig. 17). In the case of Xe, the intersystem lines Xe VII λ 995.51 Å ($5s^2\ ^1S - 5s5p\ ^3P^\circ$) and Xe VII λ 1077.12 Å ($5s5p\ ^1P^\circ - 5p^2\ ^1D$) are

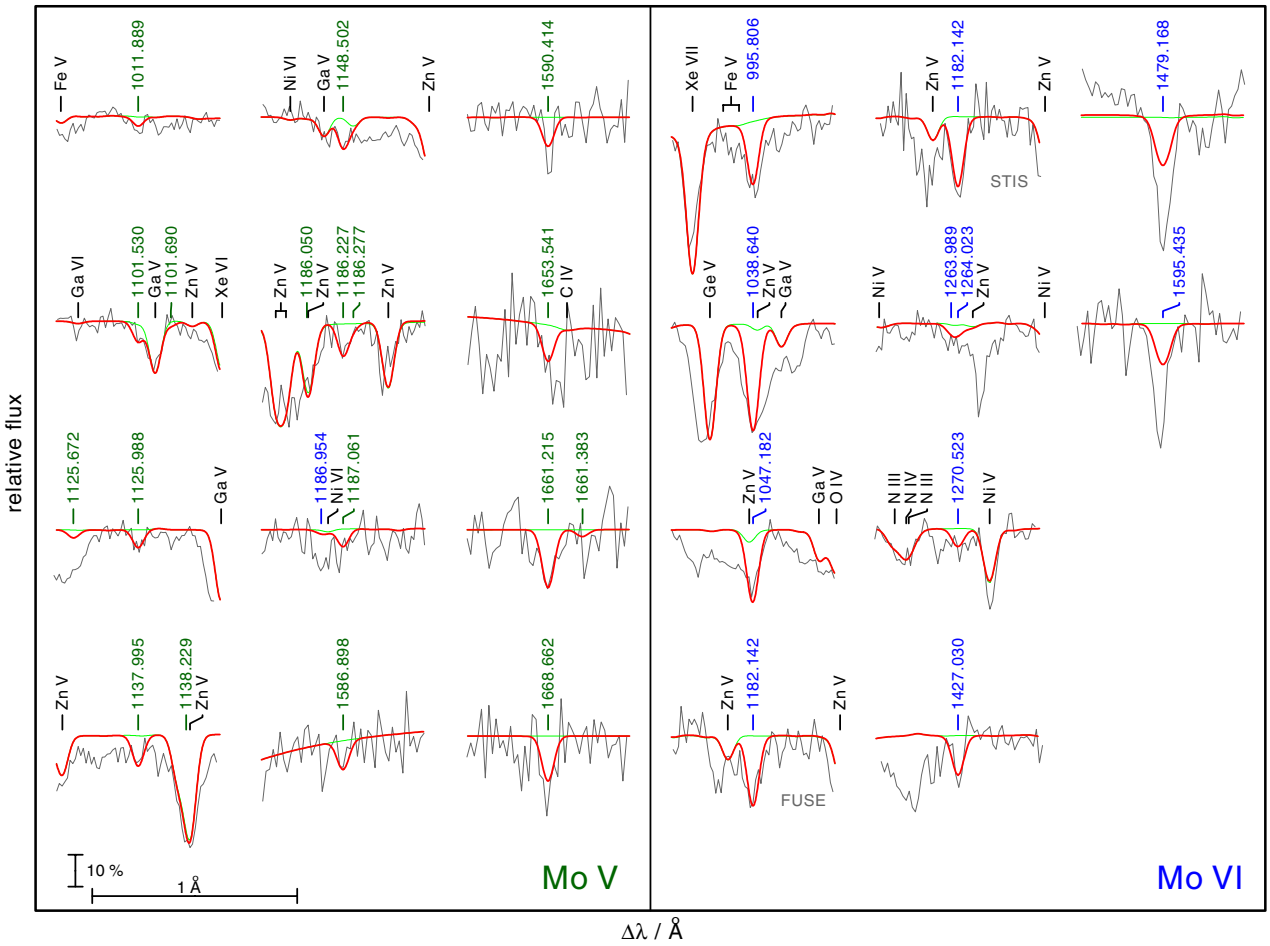

Fig. 12. Mo V lines (*left panel*, marked with their wavelengths from Table A.11 in Å, green) and Mo VI lines (*right panel*, marked blue, wavelengths from Table A.12) in the FUSE (for lines at $\lambda < 1188$ Å) and HST/STIS ($\lambda > 1188$ Å) observations of RE 0503−289. The synthetic spectra are convolved with a Gaussian (full width at half maximum = *FWHM* = 0.06 Å) to simulate the instruments' resolutions. Other identified photospheric lines are marked in black. The thick red and thin green lines show a comparison with theoretical spectra of two models with and without Mo, respectively. The vertical bar indicates 10% of the continuum flux.

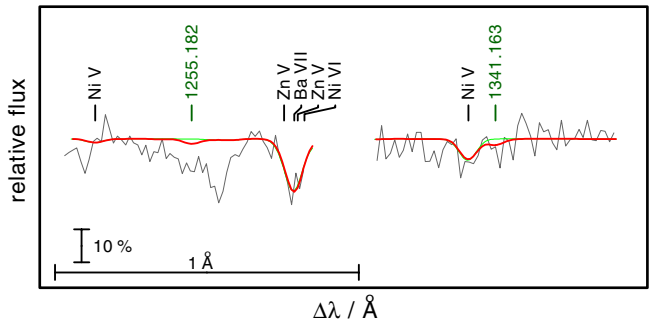

Fig. 13. Same as Fig. 12, for two Mo VII lines.

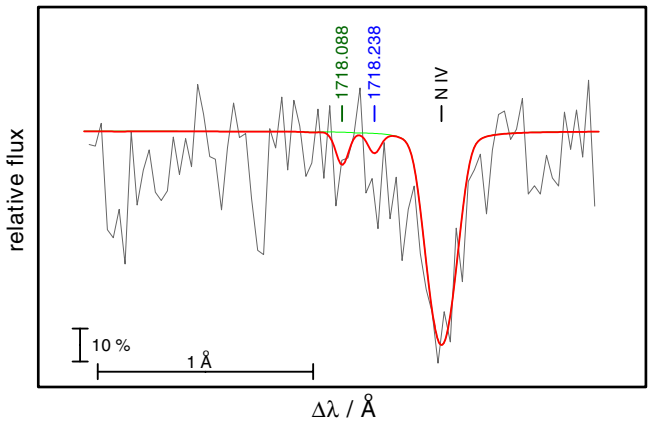

Fig. 14. Section of our HST/STIS observations of RE 0503−289 around N IV λ 1718.55 Å. The thick red and thin green lines show a comparison with theoretical spectra of two models with and without Mo, respectively. Mo V λ 1718.088 Å and Mo VI λ 1718.238 Å are marked.

very strong (Fig. 17) and require an upper Xe abundance limit of solar to fade in the noise of the observation. However, this may be strongly underestimated because of the rudimentary Xe VII model atom presently provided by TMAD. In that, only two Xe VII lines with reliable oscillator strengths are known, namely, 0.245 for Xe VII λ 995.51 Å (Kernahan et al. 1980) and 0.810 for Xe VII λ 1077.12 Å (Biémont et al. 2007). Since, for the calculation of accurate NLTE occupation numbers of the atomic levels of an specific model ion, reliable transition probabilities are mandatory for the complete ion, the Xe VII upper limit is regarded as uncertain. This issue is out of the scope of this paper but will be investigated in detail immediately after new Xe IV-VII transition probabilities become available. However, from the Xe VI lines alone, we achieve an upper limit of 1.7×10^{-7} (10 times the solar value, Fig. 17).

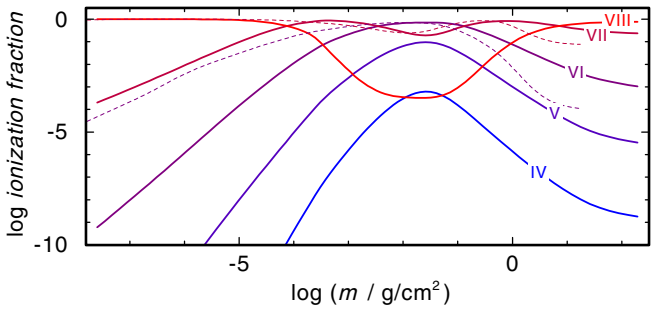

Fig. 15. Same as Fig. 10 for G191−B2B. For comparison, the dashed lines show the Mo VI+VII ionization fractions in the RE 0503−289 model.

7. Impact of diffusion on trans-iron elements

At almost the same $\log g$, RE 0503−289 has a significantly higher $T_{\rm eff}$ compared to that of G191−B2B ($T_{\rm eff}$ = 70 000 K, $\log g = 7.5$ vs. $T_{\rm eff}$ = 60 000 K, $\log g = 7.6$, respectively). Thus, the much stronger enrichment of the trans-iron elements in RE 0503−289 (Fig. 18) may be the result of a more efficient radiative levitation. Therefore, we used the NGRT[12] code (Dreizler & Wolff 1999; Schuh et al. 2002) to calculate diffusion models for both stars, using exactly the same model atoms for H, He, C, N, O, Ca, Sc, Ti, V, Cr, Mn, Fe, Co, Ni, Zn, Ga, Ge, As, Kr, Mo, Sn, Xe, and Ba, which were used for our chemically homogeneous TMAP models. For RE 0503−289, H was formally included in the calculation, but its abundance was fixed to 1.0×10^{-20}. Therefore, its contribution to the background opacity is negligible. Disregarding the fixed H abundance in RE 0503−289, the diffusion models differ only in $T_{\rm eff}$ and $\log g$.

The TMAD model atoms for As and Sn are presently rather rudimentary, especially as only a very few oscillator strengths are known. Restricting the radiative levitation calculation to include transitions with known oscillator strengths thus leads to an unrealistically small effect. We follow Rauch et al. (2013) and add all allowed line transitions in our As and Sn model atoms, using default f-values of 1. Therefore, the results of our diffusion models for these elements should be regarded as preliminary.

Figure 19 shows the calculated depth-dependent abundance profiles for Zn, Ga, Ge, As, Kr, Mo, Sn, Xe, and Ba. All these are strongly overabundant in the line-forming regions (Fig. 19). The predicted abundance profiles suggest abundance enhancements in RE 0503−289 relative to G191−B2B. This is qualitatively in agreement with the abundance patterns in Fig. 18, which were determined from our static TMAP models. However, whether it is possible to reach 2−3 dex should be demonstrated with advanced line-profile calculations in diffusive equilibrium. These would provide stringent constraints for suggested weak stellar winds (Chayer et al. 2005) and thin convective zones at the stellar surface (Chayer et al. 2015), which might impact the interplay of radiative levitation and gravitational settling.

8. Results and conclusions

With our NLTE model-atmosphere package TMAP, we calculated new models for the DO-type white dwarf RE 0503−289 with molybdenum in addition. The Mo model atoms were constructed with newly calculated Mo IV–VII oscillator strengths. We have unambiguously identified 12 Mo V and nine Mo VI lines in the observed high-resolution UV spectra of RE 0503−289.

[12] New Generation Radiative Transport.

Table 3. Same as Table 2, for G191−B2B.

Element	Mass Fraction	Number Fraction	[X]
H	9.99×10^{-1}	9.99×10^{-1}	0.132
He	$<1.98 \times 10^{-5}$	$<5.00 \times 10^{-6}$	<−4.099
C	6.31×10^{-6}	5.30×10^{-7}	−2.574
N	2.08×10^{-6}	1.50×10^{-7}	−2.522
O	1.90×10^{-5}	1.20×10^{-6}	−2.479
Al	1.12×10^{-5}	4.20×10^{-7}	−0.675
Si	5.29×10^{-5}	1.90×10^{-6}	−1.099
P	1.54×10^{-6}	5.00×10^{-8}	−0.579
S	5.72×10^{-6}	1.80×10^{-7}	−1.733
IG	1.78×10^{-6}	4.00×10^{-8}	−1.538
Fe	6.50×10^{-4}	1.17×10^{-5}	−0.269
Ni	3.84×10^{-5}	6.60×10^{-7}	−0.249
Zn	3.50×10^{-6}	5.40×10^{-8}	0.304
Ga	2.56×10^{-6}	3.70×10^{-8}	1.680
Ge	3.24×10^{-6}	4.50×10^{-8}	1.155
As	3.71×10^{-7}	5.00×10^{-9}	1.531
Kr	$<1.09 \times 10^{-6}$	$<1.31 \times 10^{-0}$	<1.000
Mo	$<5.33 \times 10^{-7}$	$<5.60 \times 10^{-9}$	<2.000
Sn	3.53×10^{-7}	3.00×10^{-9}	1.589
Xe	$<1.67 \times 10^{-7}$	$<1.28 \times 10^{-9}$	<1.000
Ba	4.00×10^{-6}	2.94×10^{-8}	2.350

The Mo V/Mo VI ionization equilibrium is well reproduced (Fig. 12). We determined a photospheric abundance of log Mo = −3.73 ± 0.2 (mass fraction 1.2−3.0 × 10^{-4}, 22 500−56 400 times the solar abundance). In addition, we determined the arsenic and tin abundances and derived log As = −5.08 ± 0.2 (0.5−1.3 × 10^{-5}, about 300−1200 times solar) and log Sn = −3.69 ± 0.2 (1.3−3.2 × 10^{-4}, about 14 300−35 200 times solar). These highly supersolar As, Mo, and Sn abundances agree well with the high abundances of other trans-iron elements in RE 0503−289 (Fig. 18).

G191−B2B does not exhibit Kr, Mo, and Xe lines in its UV spectrum. We investigated the strongest lines in the model and found upper limits for the abundances of Kr (1.1×10^{-6}, 10 times solar), Mo (5.3×10^{-7}, 100 times solar), and Xe (1.7×10^{-7}, 10 times solar). Whether radiative levitation yields abundances of these elements that are consistent with observations should be demonstrated with advanced line-profile calculations in diffusive equilibrium, as depicted in Fig. 19. In addition, we determined the arsenic abundance and derived log As = −6.43 ± 0.2 (2.3−5.9 × 10^{-7}, about 21−53 times solar).

The computation of reliable transition probabilities for Mo IV–VII was a prerequisite for the identification of Mo lines and the subsequent abundance determination. The hitherto known abundance pattern of RE 0503−289 (Fig. 18) indicates that other yet unidentified species should be detectable. Therefore, the precise evaluation of their laboratory spectra, i.e., the measurement of line wavelengths and strengths, as well as the determination of level energies and the subsequent calculation of transition probabilities are absolutely essential.

The example of the arsenic abundance determination (Sect. 6.1) had demonstrated that state-of-the-art NLTE stellar-atmosphere models are mandatory for the precise spectral analysis of hot stars.

Acknowledgements. T.R. and D H. are supported by the German Aerospace Center (DLR, grants 05 OR 1402 and 50 OR 1501, respectively). The GAVO project had been supported by the Federal Ministry of Education and Research (BMBF) at Tübingen (05 AC 6 VTB, 05 AC 11 VTB) and is funded at Heidelberg

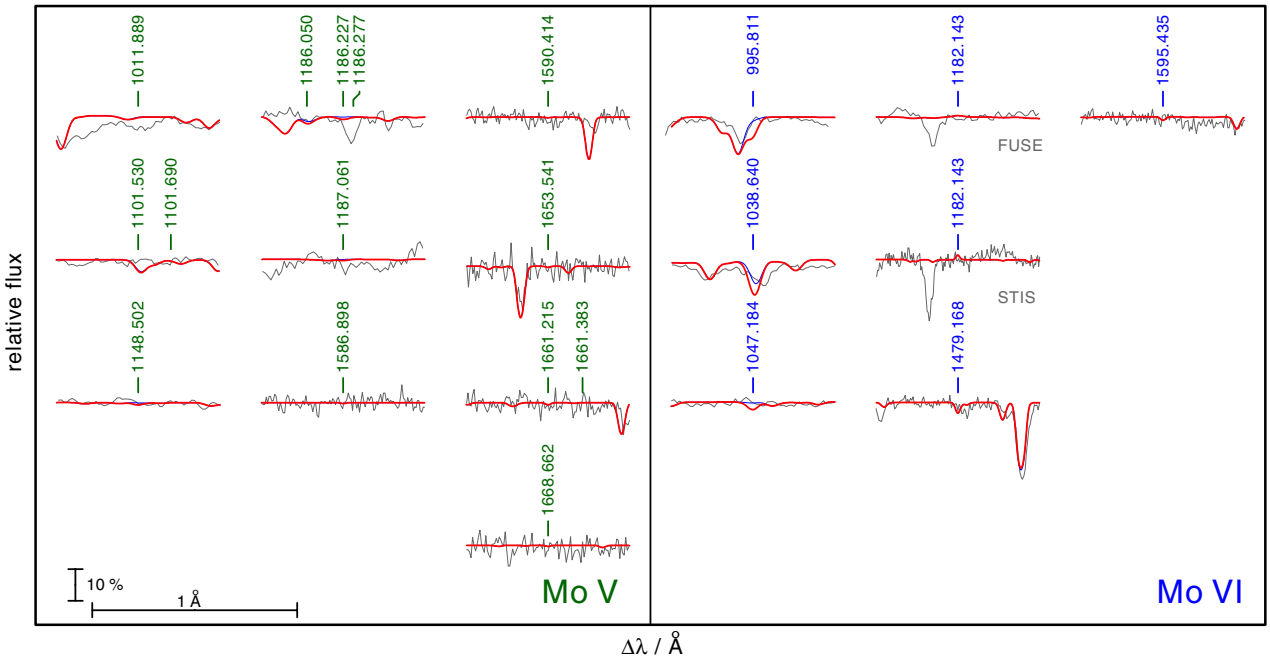

Fig. 16. Like Fig. 12 for G191−B2B. The thick red and thin blue spectra are calculated from models with photospheric Mo abundances of 5.3×10^{-6} and 5.3×10^{-7} (mass fractions, about 1000 and 100 times the solar value), respectively.

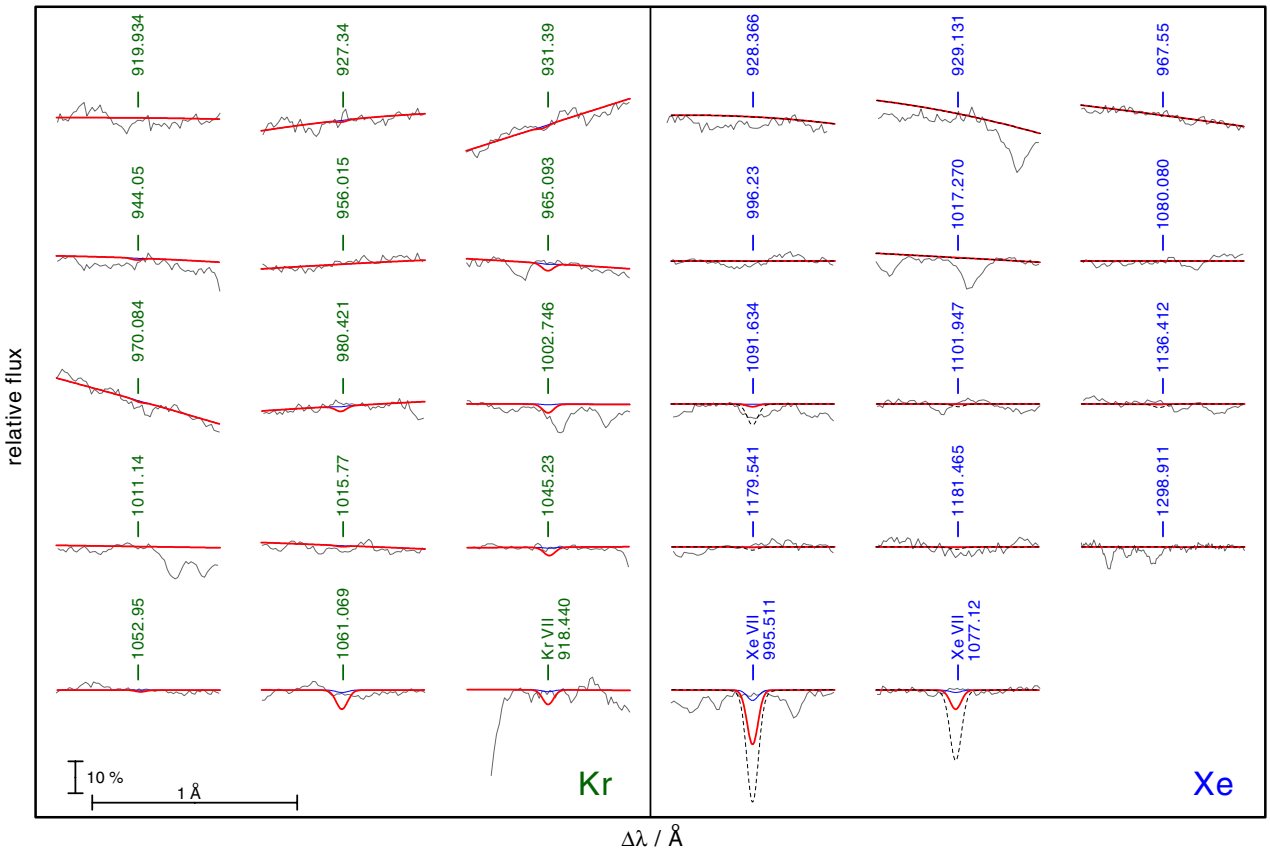

Fig. 17. Theoretical line profiles of Kr (*left panel*, 14 Kr VI lines and 1 Kr VII line) and Xe (*right panel*, 12 Xe VI and 2 Xe VII lines) compared to the observations of G191−B2B. The spectra are calculated from models with photospheric abundances (mass fractions) of Kr: 1.1×10^{-5} (thick red, 100 times solar) and 1.1×10^{-6} (thin blue, 10 times solar) and of Xe: 1.7×10^{-6} (dashed black, 100 times solar), 1.7×10^{-7} (thick red, 10 times solar), and 1.7×10^{-8} (thin blue, solar).

(05 AC 11 VH3). Financial support from the Belgian FRS-FNRS is also acknowledged. P.Q. is research director of this organization. We thank our referee, Stéphane Vennes, for constructive criticism. Some of the data presented in this paper were obtained from the Mikulski Archive for Space Telescopes (MAST). STScI is operated by the Association of Universities for Research in Astronomy, Inc., under NASA contract NAS5-26555. Support for MAST for non-HST data is provided by the NASA Office of Space Science via grant NNX09AF08G and by other grants and contracts. This research has made use of NASA's Astrophysics

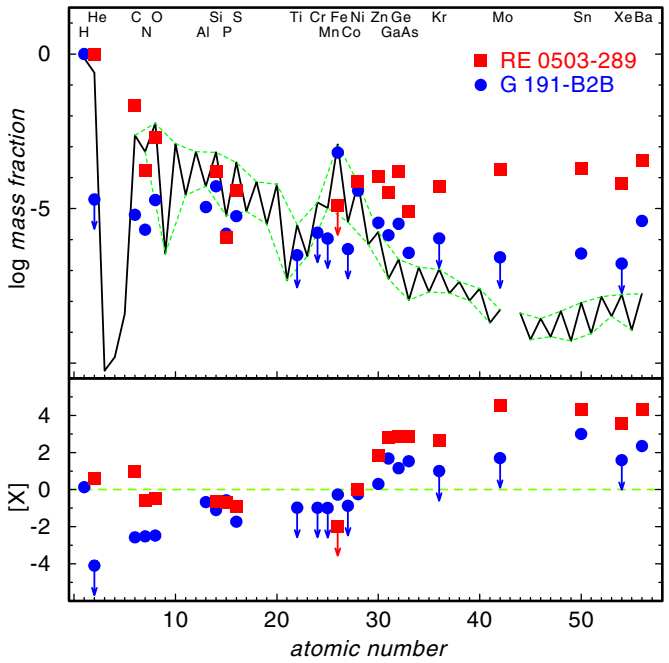

Fig. 18. Solar abundances (Asplund et al. 2009; Scott et al. 2015b,a; Grevesse et al. 2015, thick line; the dashed green lines connect the elements with even and with odd atomic number) compared with the determined photospheric abundances of G191−B2B (blue circles, Rauch et al. 2013) and RE 0503−289 (red squares, Dreizler & Werner 1996; Werner et al. 2012b; Rauch et al. 2013, 2014a,b, 2015a,b, and this work). *Top panel*: abundances given as logarithmic mass fractions. Arrows indicate upper limits. *Bottom panel*: abundance ratios to respective solar values, [X] denotes log (fraction/solar fraction) of species X. The dashed green line indicates solar abundances.

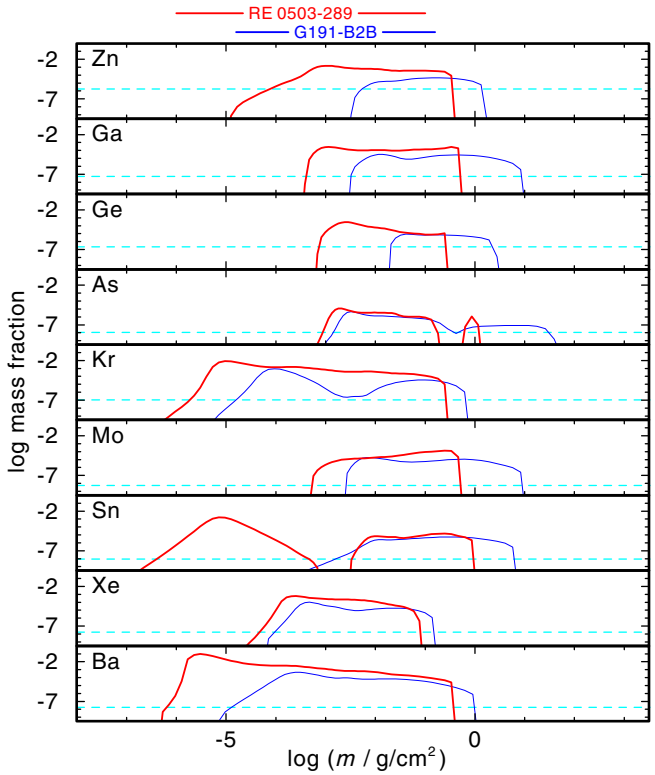

Fig. 19. Abundance profiles in our diffusion models for G191−B2B (thin blue) and RE 0503−289 (thick red). The dashed, horizontal lines indicate solar abundance values. The formation regions of UV lines in both models are indicated at the top.

Data System and the SIMBAD database, operated at CDS, Strasbourg, France. The TOSS service (http://dc.g-vo.org/TOSS) that provides weighted oscillator strengths and transition probabilities was constructed as part of the activities of the German Astrophysical Virtual Observatory.

References

Asplund, M., Grevesse, N., Sauval, A. J., & Scott, P. 2009, ARA&A, 47, 481
Biémont, É., Clar, M., Fivet, V., et al. 2007, Eur. Phys. J. D, 44, 23
Cabeza, M. I., Iglesias, L., Rico, F. R., & Kaufman, V. 1989, Phys. Scr, 40, 457
Chayer, P., Vennes, S., Dupuis, J., & Kruk, J. W. 2005, ApJ, 630, L169
Chayer, P., Dupuis, J., & Kruk, J. W. 2015, in 19th European Workshop on White Dwarfs, eds. P. Dufour, P. Bergeron, & G. Fontaine, ASP Conf. Ser., 493, 3
Cowan, R. D. 1981, The theory of atomic structure and spectra (Berkeley, CA: University of California Press)
Cowley, C. R. 1970, The theory of stellar spectra (New York: Gordon & Breach)
Cowley, C. R. 1971, The Observatory, 91, 139
Curtis, L. J., & Theodosiou, C. E. 1989, Phys. Rev. A, 39, 605
Dowler, P., Rixon, G., & Tody, D. 2010, Table Access Protocol Version 1.0, IVOA Recommendation
Dreizler, S., & Werner, K. 1996, A&A, 314, 217
Dreizler, S., & Wolff, B. 1999, A&A, 348, 189
Fischer, C. F. 1977, J. Phys. B, 10, 1241
Fraga, S., Karwowski, J., & Saxena, K. M. S. 1976, Handbook of Atomic Data (Amsterdam: Elsevier)
Grevesse, N., Scott, P., Asplund, M., & Sauval, A. J. 2015, A&A, 573, A27
Hubeny, I., Hummer, D. G., & Lanz, T. 1994, A&A, 282, 151
Hummer, D. G., & Mihalas, D. 1988, ApJ, 331, 794
Johnson, W. R., Kolb, D., & Huang, K.-N. 1983, Atomic Data and Nuclear Data Tables, 28, 333
Kernahan, J. A., Pinnington, E. H., O'Neill, J. A., Bahr, J. L., & Donnelly, K. E. 1980, J. Opt. Soc. Am., 70, 1126
McCook, G. P., & Sion, E. M. 1999a, ApJS, 121, 1
McCook, G. P., & Sion, E. M. 1999b, VizieR Online Data Catalog: III/210
Migdalek, J., & Baylis, W. E. 1979, J. Phys. B, 12, 1113
Moore, C. E. 1958, Atomic Energy Levels as Derived from the Analysis of Optical Spectra Molybdenum through Lanthanum and Hafnium through Actinium (NIST)
Morton, D. C. 2000, ApJS, 130, 403
Osuna, P., Barbarisi, I., Salgado, J., & Arviset, C. 2005, in Astronomical Data Analysis Software and Systems XIV, eds. P. Shopbell, M. Britton, & R. Ebert, ASP Conf. Ser., 347, 198
Osuna, P., Guainazzi, M., Salgado, J., Dubernet, M.-L., & Roueff, E. 2010, Simple Spectral Lines Data Model, IVOA Recommendation 2 Dec
Pinnington, E. H., Bahr, J. L., Kernahan, J. A., & Irwin, D. J. G. 1981, J. Phys. B, 14, 1291
Quinet, P., Palmeri, P., Biémont, E., et al. 1999, MNRAS, 307, 934
Quinet, P., Palmeri, P., Biémont, E., et al. 2002, J. Alloys Comp., 344, 255
Rauch, T. 2012, ArXiv e-prints [arXiv:1210.7636]
Rauch, T., & Deetjen, J. L. 2003, in Stellar Atmosphere Modeling, eds. I. Hubeny, D. Mihalas, & K. Werner, ASP Conf. Ser., 288, 103
Rauch, T., Werner, K., Biémont, É., Quinet, P., & Kruk, J. W. 2012, A&A, 546, A55
Rauch, T., Werner, K., Bohlin, R., & Kruk, J. W. 2013, A&A, 560, A106
Rauch, T., Werner, K., Quinet, P., & Kruk, J. W. 2014a, A&A, 564, A41
Rauch, T., Werner, K., Quinet, P., & Kruk, J. W. 2014b, A&A, 566, A10
Rauch, T., Hoyer, D., Quinet, P., Gallardo, M., & Raineri, M. 2015a, A&A, 577, A88
Rauch, T., Werner, K., Quinet, P., & Kruk, J. W. 2015b, A&A, 577, A6
Reader, J. 2010, J. Phys. B, 43, 074024
Reader, J., & Tauheed, A. 2015, J. Phys B, 48, 144001
Salgado, J., Osuna, P., Guainazzi, M., et al. 2010, Simple Line Access Protocol, IVOA http://www.ivoa.net/documents/SLAP/
Schuh, S. L., Dreizler, S., & Wolff, B. 2002, A&A, 382, 164
Scott, P., Asplund, M., Grevesse, N., Bergemann, M., & Sauval, A. J. 2015a, A&A, 573, A26
Scott, P., Grevesse, N., Asplund, M., et al. 2015b, A&A, 573, A25
Shirai, T., Sugar, J., Musgrove, A., & Wiese, W. L. 2000, Spectral Data for Highly Ionized Atoms: Ti, V, Cr, Mn, Fe, Co, Ni, Cu, Kr, and Mo (AIP)
Sugar, J., & Musgrove, A. 1988, J. Phys. Chem. Ref. Data, 17, 155
Vennes, S., & Lanz, T. 2001, ApJ, 553, 399
Werner, K., Deetjen, J. L., Dreizler, S., et al. 2003, in Stellar Atmosphere Modeling, eds. I. Hubeny, D. Mihalas, & K. Werner, ASP Conf. Ser., 288, 31
Werner, K., Dreizler, S., & Rauch, T. 2012a, TMAP: Tübingen NLTE Model-Atmosphere Package (Astrophysics Source Code Library)
Werner, K., Rauch, T., Ringat, E., & Kruk, J. W. 2012b, ApJ, 753, L7

Appendix A: Additional tables

Table A.1. Radial parameters (in cm^{-1}) adopted for the calculations in Mo IV.

Configuration	Parameter	HFR	Fitted	Ratio	Note[a]
		Even parity			
$4d^3$	E_{av}	17 281	16 028		
	F^2(4d, 4d)	63 593	53 099	0.835	
	F^4(4d, 4d)	41 828	36 184	0.865	
	α	0	9		
	β	0	−491		
	ζ_{4d}	812	810	0.997	
$4d^25s$	E_{av}	75 210	73 187		
	F^2(4d, 4d)	66 028	53 488	0.810	
	F^4(4d, 4d)	43 601	36 324	0.833	
	α	0	30		
	β	0	−417		
	ζ_{4d}	878	875	0.996	
	G^2(4d, 5s)	15 995	14 485	0.906	
$4d^26s$	E_{av}	201 514	200 119		
	F^2(4d, 4d)	67 245	53 932	0.802	
	F^4(4d, 4d)	44 505	35 007	0.787	
	α	0	45		
	β	0	−420		F
	ζ_{4d}	904	924	1.023	
	G^2(4d, 6s)	3356	2624	0.782	
$4d^25d$	E_{av}	193 759	193 316		
	F^2(4d, 4d)	67 204	54 471	0.811	
	F^4(4d, 4d)	44 476	36 658	0.824	
	α	0	31		
	β	0	−256		
	ζ_{4d}	903	924	1.024	
	ζ_{5d}	139	150	1.077	
	F^2(4d, 5d)	14 772	12 432	0.842	
	F^4(4d, 5d)	6861	5749	0.838	
	G^0(4d, 5d)	4764	3206	0.673	
	G^2(4d, 5d)	5093	3789	0.744	
	G^4(4d, 5d)	4081	3439	0.843	
		Odd parity			
$4d^25p$	E_{av}	125 149	124 281		
	F^2(4d, 4d)	66 425	53 851	0.811	
	F^4(4d, 4d)	43 895	36 220	0.825	
	α	0	33		
	β	0	−333		
	ζ_{4d}	888	930	1.048	
	ζ_{5p}	1801	2130	1.183	
	F^2(4d, 5p)	25 420	23 019	0.906	
	G^1(4d, 5p)	9987	9357	0.937	
	G^3(4d, 5p)	8792	8106	0.922	

Notes. [a] F is a parameter fixed in the fitting process.

Table A.2. Radial parameters (in cm^{-1}) adopted for the calculations in Mo V.

Configuration	Parameter	HFR	Fitted	Ratio	Note[a]
		Even parity			
$4d^2$	E_{av}	16 700	15 960		
	F^2(4d, 4d)	67 562	55 311	0.819	
	F^4(4d, 4d)	44 738	35 260	0.788	
	α	0	76		
	β	0	−166		
	ζ_{4d}	911	920	1.009	
4d5s	E_{av}	104 520	99 547		
	ζ_{4d}	976	982	1.005	
	G^2(4d, 5s)	16 390	14 551	0.888	
4d6s	E_{av}	263 493	256 257		
	ζ_{4d}	1003	1022	1.019	
	G^2(4d, 6s)	3729	3106	0.833	
4d5d	E_{av}	245 631	239 792		
	ζ_{4d}	1001	1016	1.015	
	ζ_{5d}	198	234	1.178	
	F^2(4d, 5d)	18 455	15 120	0.819	
	F^4(4d, 5d)	8872	7388	0.833	
	G^0(4d, 5d)	5787	4043	0.699	
	G^2(4d, 5d)	6372	5106	0.801	
	G^4(4d, 5d)	5194	4146	0.798	
4d5g	E_{av}	335 286	329 641		
	ζ_{4d}	1012	1031	1.019	
	ζ_{5g}	1	1	1.000	F
	F^2(4d, 5g)	6192	5389	0.870	
	F^4(4d, 5g)	1861	1707	0.918	
	G^2(4d, 5g)	1063	1139	1.071	R1
	G^4(4d, 5g)	704	753	1.071	R1
	G^6(4d, 5g)	518	555	1.071	R1
$5s^2$	E_{av}	213 688	204 228		
$5p^2$	E_{av}	332 119	323 949		
	F^2(5p, 5p)	39 738	41 118	1.035	
	α	0	−621		
	ζ_{5p}	2540	3202	1.260	
5s5d	E_{av}	357 810	349 503		
	ζ_{5d}	219	219	1.000	F
	G^2(5s, 5d)	19 094	17 185	0.900	F
5s6s	E_{av}	376 977	370 379		
	G^0(5s, 6s)	3641	3277	0.900	F
		Odd parity			
4d5p	E_{av}	162 256	157 254		
	ζ_{4d}	985	1075	1.091	R2
	ζ_{5p}	2318	2813	1.213	
	F^2(4d, 5p)	28 585	23 914	0.837	
	G^1(4d, 5p)	10 632	10 070	0.947	
	G^3(4d, 5p)	9701	8409	0.867	
4d6p	E_{av}	287 398	280 416		
	ζ_{4d}	1004	1096	1.091	R2
	ζ_{6p}	971	1179	1.214	
	F^2(4d, 6p)	10 594	8043	0.759	
	G^1(4d, 6p)	2868	1938	0.675	R3
	G^3(4d, 6p)	2956	1995	0.675	R3
4d4f	E_{av}	256 786	251 161		
	ζ_{4d}	988	1077	1.091	R2
	ζ_{4f}	8	8	1.000	F
	F^2(4d, 4f)	31 387	26 142	0.832	
	F^4(4d, 4f)	17 861	14 862	0.832	
	G^1(4d, 4f)	31 404	28 322	0.901	
	G^3(4d, 4f)	18 764	16 912	0.901	
	G^5(4d, 4f)	13 035	11 745	0.901	

Notes. [(a)] F: fixed parameter value; R1, R2, R3: ratios of these parameters were fixed in the fitting process.

Table A.2. continued.

Configuration	Parameter	HFR	Fitted	Ratio	Note[a]
4d5f	E_{av}	325 720	319 198		
	ζ_{4d}	1001	1092	1.091	R2
	ζ_{5f}	5	5	1.000	F
	F^2(4d, 5f)	13 834	11 607	0.839	
	F^4(4d, 5f)	7809	6547	0.838	
	G^1(4d, 5f)	13 741	12 541	0.913	
	G^3(4d, 5f)	8630	7867	0.912	
	G^5(4d, 5f)	6115	5570	0.911	
4d6f	E_{av}	363 451	356 835		
	ζ_{4d}	1007	1099	1.091	R2
	ζ_{6f}	3	3	1.000	F
	F^2(4d, 6f)	7186	6050	0.842	
	F^4(4d, 6f)	4053	3412	0.842	
	G^1(4d, 6f)	6893	6546	0.950	
	G^3(4d, 6f)	4448	4073	0.916	
	G^5(4d, 6f)	3186	2917	0.915	
4d7f	E_{av}	386 059	378 193		
	ζ_{4d}	1010	1102	1.091	R2
	ζ_{7f}	2	2	1.000	F
	F^2(4d, 7f)	4217	3557	0.843	
	F^4(4d, 7f)	2381	2009	0.844	
	G^1(4d, 7f)	3939	3621	0.919	
	G^3(4d, 7f)	2584	2373	0.918	
	G^5(4d, 7f)	1863	1711	0.918	
4d8f	E_{av}	400 596	392 685		
	ζ_{4d}	1011	1103	1.091	R2
	ζ_{8f}	1	1	1.000	F
	F^2(4d, 8f)	2691	2272	0.844	
	F^4(4d, 8f)	1522	1285	0.844	
	G^1(4d, 8f)	2466	2271	0.921	
	G^3(4d, 8f)	1635	1503	0.919	
	G^5(4d, 8f)	1185	1088	0.918	
4d9f	E_{av}	410 472	404 023		
	ζ_{4d}	1012	1104	1.091	R2
	ζ_{9f}	1	1	1.000	F
	F^2(4d, 9f)	1825	1552	0.850	F
	F^4(4d, 9f)	1033	879	0.850	F
	G^1(4d, 9f)	1650	1326	0.800	F
	G^3(4d, 9f)	1102	884	0.800	F
	G^5(4d, 9f)	801	642	0.800	F
5s5p	E_{av}	265 407	258 722		
	ζ_{5p}	2565	2961	1.154	
	G^1(5s, 5p)	50 976	39 056	0.766	
5s4f	E_{av}	365 788	356 759		
	ζ_{4f}	11	11	1.000	F
	G^3(5s, 4f)	28 615	23 484	0.821	
$4p^5 4d^3$	E_{av}	340 658	329 068		
	F^2(4d, 4d)	68 193	53 949	0.791	
	F^4(4d, 4d)	45 181	37 828	0.837	
	α	0	−10		
	β	0	−127		
	ζ_{4p}	13 353	13 445	1.007	
	ζ_{4d}	936	878	0.938	
	F^2(4p, 4d)	73 694	64 641	0.877	
	G^1(4p, 4d)	92 191	71 050	0.771	
	G^3(4p, 4d)	56 862	47 299	0.832	

Table A.3. Radial parameters (in cm^{-1}) adopted for the calculations in Mo VI.

Configuration	Parameter	HFR	Fitted	Ratio	Note[a]
		Even parity			
4d	E_{av}	6940	6979		
	ζ_{4d}	1014	1040	1.026	
5d	E_{av}	289 239	285 322		
	ζ_{5d}	264	303	1.148	
6d	E_{av}	391 958	387 186		
	ζ_{6d}	126	146	1.161	
7d	E_{av}	444 684	440 130		
	ζ_{7d}	71	83	1.170	
8d	E_{av}	475 734	471 318		
	ζ_{8d}	44	52	1.175	
5s	E_{av}	126 902	124 312		
6s	E_{av}	319 460	314 126		
7s	E_{av}	405 700	400 898		
8s	E_{av}	452 302	447 811		
5g	E_{av}	399 240	395 878		
	ζ_{5g}	1.4	1.4	1.000	F
6g	E_{av}	448 202	444 402		
	ζ_{6g}	0.7	0.7	1.000	F
7g	E_{av}	477 706	473 769		
	ζ_{7g}	0.4	0.4	1.000	F
8g	E_{av}	496 846	492 842		
	ζ_{8g}	0.3	0.3	1.000	F
7i	E_{av}	478 466	474 434		
	ζ_{7i}	0.2	0.2	1.000	F
8i	E_{av}	497 360	493 348		
	ζ_{8i}	0.1	0.1	1.000	F
		Odd parity			
5p	E_{av}	191 999	189 199		
	ζ_{5p}	2857	3301	1.155	
6p	E_{av}	347 659	342 627		
	ζ_{6p}	1255	1382	1.102	
7p	E_{av}	420 512	415 898		
	ζ_{7p}	667	691	1.037	
8p	E_{av}	461 055	456 619		
	ζ_{8p}	397	407	1.024	
9p	E_{av}	486 031	481 747		
	ζ_{9p}	256	289	1.129	
10p	E_{av}	502 531	498 326		
	ζ_{10p}	174	179	1.024	
11p	E_{av}	514 002	509 824		
	ζ_{11p}	124	130	1.043	
4f	E_{av}	283 752	279 178		
	ζ_{4f}	15	15	1.000	F
5f	E_{av}	384 116	378 130		
	ζ_{5f}	10	10	1.000	F
6f	E_{av}	439 000	433 239		
	ζ_{6f}	5.7	5.7	1.000	F
7f	E_{av}	471 803	466 996		
	ζ_{7f}	3.6	3.6	1.000	F
8f	E_{av}	492 861	488 364		
	ζ_{8f}	2.4	2.4	1.000	F
9f	E_{av}	507 147	502 815		
	ζ_{9f}	1.7	1.7	1.000	F
6h	E_{av}	449 115	445 105		
	ζ_{6h}	0.5	0.5	1.000	F
7h	E_{av}	478 275	474 297		
	ζ_{7h}	0.3	0.3	1.000	F
8h	E_{av}	497 230	493 247		
	ζ_{8h}	0.2	0.2	1.000	F
8k	E_{av}	497 392	493 378		
	ζ_{8k}	0.1	0.1	1.000	F

Notes. [(a)] F: fixed parameter value; R1, R2, R3: ratios of these parameters were fixed in the fitting process.

Table A.3. continued.

Configuration	Parameter	HFR	Fitted	Ratio	Note[a]
$4p^5 4d^2$	E_{av}	335 899	328 744		
	F^2(4d, 4d)	71 670	59 093	0.824	
	F^4(4d, 4d)	47 745	38 616	0.809	
	α	0	17		
	β	0	−420		
	ζ_{4p}	13 848	14 202	1.026	
	ζ_{4d}	1037	1037	1.000	F
	F^2(4p, 4d)	76 913	66 050	0.859	
	G^1(4p, 4d)	96 524	77 164	0.799	
	G^3(4p, 4d)	59 818	49 326	0.825	
$4p^5 4d5s$	E_{av}	457 444	450 131		
	ζ_{4p}	14 235	14 483	1.017	
	ζ_{4d}	1101	1129	1.025	
	F^2(4p, 4d)	78 673	66 507	0.845	
	G^1(4p, 4d)	98 887	88 998	0.900	F
	G^3(4p, 4d)	61 423	55 280	0.900	F
	G^1(4p, 5s)	8984	7014	0.781	
	G^2(4d, 5s)	16 675	13 729	0.823	
4f – $4p^5 4d^2$	R^1(4p, 4f;4d, 4d)	62 948	54 136	0.860	R1
	R^3(4p, 4f;4d, 4d)	36 931	31 762	0.860	R1
5f – $4p^5 4d^2$	R^1(4p, 5f;4d, 4d)	38 112	29 914	0.785	R2
	R^3(4p, 5f;4d, 4d)	23 989	18 829	0.785	R2
6f – $4p^5 4d^2$	R^1(4p, 6f;4d, 4d)	25 591	23 426	0.915	R3
	R^3(4p, 6f;4d, 4d)	16 592	15 188	0.915	R3

Table A.4. Radial parameters (in cm^{-1}) adopted for the calculations in Mo VII.

Configuration	Parameter	HFR	Fitted	Ratio	Note[a]
		Even parity			
$4p^6$	E_{av}	0	21 119		
$4p^5 5p$	E_{av}	561 281	562 851		
	ζ_{4p}	14 921	15 363	1.030	
	ζ_{5p}	3488	4002	1.147	
	$F^2(4p, 5p)$	29 857	24 371	0.816	
	$G^0(4p, 5p)$	6158	5332	0.866	
	$G^2(4p, 5p)$	8430	7935	0.941	
$4p^5 4f$	E_{av}	639 783	641 540		
	ζ_{4p}	14 771	15 580	1.055	
	ζ_{4f}	26	26	1.000	F
	$F^2(4p, 4f)$	50 260	41 550	0.827	
	$G^2(4p, 4f)$	39 595	38 768	0.979	
	$G^4(4p, 4f)$	26 564	22 964	0.864	
$4p^5 5f$	E_{av}	779 673	777 325		
	ζ_{4p}	14 910	14 839	0.995	
	ζ_{5f}	16	16	1.000	F
	$F^2(4p, 5f)$	20 061	18 055	0.900	F
	$G^2(4p, 5f)$	14 898	13 408	0.900	F
	$G^4(4p, 5f)$	10 403	9363	0.900	F
$4s4p^6 4d$	E_{av}	598 938	600 309		
	ζ_{4d}	1152	1080	0.938	
	$G^2(4s, 4d)$	75 275	69 544	0.924	
$4p^4 4d^2$	E_{av}	677 980	676 885		
	ζ_{4p}	14 606	15 080	1.032	
		Odd parity			
$4p^5 4d$	E_{av}	333 514	338 837		
	ζ_{4p}	14 422	14 556	1.009	
	ζ_{4d}	1135	1208	1.063	
	$F^2(4p, 4d)$	79 809	71 884	0.901	
	$G^1(4p, 4d)$	100 362	83 374	0.831	
	$G^3(4p, 4d)$	62 451	56 668	0.907	
$4p^5 5d$	E_{av}	671 346	672 809		
	ζ_{4p}	14 913	15 411	1.033	
	ζ_{5d}	334	377	1.127	
	$F^2(4p, 5d)$	22 803	18 791	0.824	
	$G^1(4p, 5d)$	11 320	8210	0.725	
	$G^3(4p, 5d)$	8658	7930	0.916	
$4p^5 5s$	E_{av}	488 570	491 951		
	ζ_{4p}	14 829	15 316	1.033	
	$G^1(4p, 5s)$	9721	8535	0.878	
$4p^5 6s$	E_{av}	717 058	717 580		
	ζ_{4p}	14 952	15 422	1.031	
	$G^1(4p, 6s)$	3153	2754	0.874	
$4p^5 7s$	E_{av}	823 026	824 426		
	ζ_{4p}	14 988	14 988	1.000	F
	$G^1(4p, 7s)$	1479	1331	0.900	F
$4p^5 8s$	E_{av}	881 412	882 412		
	ζ_{4p}	15 003	15 003	1.000	F
	$G^1(4p, 8s)$	826	743	0.900	F
$4p^5 9s$	E_{av}	917 112	918 112		
	ζ_{4p}	15 010	15 010	1.000	F
	$G^1(4p, 9s)$	511	460	0.900	F
$4p^5 10s$	E_{av}	940 560	941 960		
	ζ_{4p}	15 015	15 015	1.000	F
	$G^1(4p, 10s)$	339	305	0.900	F
$4p^5 5g$	E_{av}	801 642	804 198		
	ζ_{4p}	15 014	15 478	1.031	
	ζ_{5g}	2.2	2.2	1.000	F
	$F^2(4p, 5g)$	10 237	9359	0.914	
	$G^3(4p, 5g)$	1612	2007	1.245	
	$G^5(4p, 5g)$	1141	1090	0.955	
$4s4p^6 5p$	E_{av}	831 694	831 323		
	ζ_{5p}	3501	3501	1.000	F
	$G^1(4s, 5p)$	8838	8527	0.965	

Notes. [(a)] F: fixed parameter value.

Table A.5. Comparison between available experimental and calculated energy levels in Mo IV. Energies are given in cm^{-1}.

E_{exp} [a]	E_{calc} [b]	ΔE	J	Leading components (in %) in LS coupling[c]
				Even parity
0.00	−34	34	1.5	99 $4d^3\ ^4F$
778.02	742	36	2.5	99 $4d^3\ ^4F$
1759.76	1716	44	3.5	99 $4d^3\ ^4F$
2864.58	2817	48	4.5	98 $4d^3\ ^4F$
10 330.59	10 370	−39	1.5	82 $4d^3\ ^4P$ + 16 $4d^3\ ^2P$
10 337.77	10 414	−76	0.5	92 $4d^3\ ^4P$ + 8 $4d^3\ ^2P$
11 580.50	11 661	−80	3.5	99 $4d^3\ ^2G$
11 611.99	11 688	−76	2.5	99 $4d^3\ ^4P$
12 310.80	12 366	−55	4.5	83 $4d^3\ ^2G$ + 15 $4d^3\ ^2H$
14 175.62	14 146	30	1.5	47 $4d^3\ ^2P$ + 27 $4d^3\ ^2D$ + 17 $4d^3\ ^4P$
14 347.72	14 124	224	0.5	91 $4d^3\ ^2P$ + 8 $4d^3\ ^4P$
15 995.13	15 989	6	4.5	85 $4d^3\ ^2H$ + 15 $4d^3\ ^2G$
16 357.48	16 326	31	5.5	100 $4d^3\ ^2H$
16 809.32	17 007	−198	2.5	80 $4d^3\ ^2D$ + 17 $4d^3\ ^2D$
17 107.35	17 117	−10	1.5	46 $4d^3\ ^2D$ + 36 $4d^3\ ^2P$ + 14 $4d^3\ ^2D$
24 787.03	24 769	18	3.5	99 $4d^3\ ^2F$
25 100.40	25 075	25	2.5	98 $4d^3\ ^2F$
38 922.29	38 877	45	2.5	80 $4d^3\ ^2D$ + 18 $4d^3\ ^2D$
39 230.53	39 234	−3	1.5	76 $4d^3\ ^2D$ + 23 $4d^3\ ^2D$
60 896.28	60 933	−37	1.5	99 $4d^2(^3F)5s\ ^4F$
61 626.19	61 665	−39	2.5	98 $4d^2(^3F)5s\ ^4F$
62 708.50	62 744	−35	3.5	99 $4d^2(^3F)5s\ ^4F$
64 046.46	64 077	−31	4.5	99 $4d^2(^3F)5s\ ^4F$
69 178.07	69 126	52	2.5	93 $4d^2(^3F)5s\ ^2F$
71 358.31	71 265	93	3.5	97 $4d^2(^3F)5s\ ^2F$
71 750.36	71 680	70	0.5	99 $4d^2(^3P)5s\ ^4P$
72 162.82	72 103	60	1.5	93 $4d^2(^3P)5s\ ^4P$ + 6 $4d^2(^1D)5s\ ^2D$
72 236.20	72 217	19	2.5	72 $4d^2(^3P)5s\ ^4P$ + 25 $4d^2(^1D)5s\ ^2D$
74 008.77	74 019	−10	1.5	89 $4d^2(^1D)5s\ ^2D$ + 6 $4d^2(^3P)5s\ ^4P$
74 981.08	74 977	4	2.5	69 $4d^2(^1D)5s\ ^2D$ + 27 $4d^2(^3P)5s\ ^4P$
79 106.26	79 132	−26	4.5	99 $4d^2(^1G)5s\ ^2G$
79 193.56	79 168	26	3.5	98 $4d^2(^1G)5s\ ^2G$
79 898.80	79 976	−77	0.5	97 $4d^2(^3P)5s\ ^2P$
81 052.21	81 122	−70	1.5	95 $4d^2(^3P)5s\ ^2P$
99 783.80	99 784	0	0.5	98 $4d^2(^1S)5s\ ^2S$
180 788.80	180 803	−14	2.5	64 $4d^2(^3F)5d\ ^4G$ + 32 $4d^2(^3F)5d\ ^2F$
181 502.72	181 458	45	3.5	69 $4d^2(^3F)5d\ ^4H$ + 24 $4d^2(^3F)5d\ ^4G$
182 001.68	182 007	−5	2.5	52 $4d^2(^3F)5d\ ^2F$ + 33 $4d^2(^3F)5d\ ^4G$ + 6 $4d^2(^3F)5d\ ^4D$
182 009.98	182 053	−43	0.5	76 $4d^2(^3F)5d\ ^4D$ + 18 $4d^2(^3F)5d\ ^2P$
182 139.47	182 091	48	3.5	72 $4d^2(^3F)5d\ ^4G$ + 22 $4d^2(^3F)5d\ ^4H$
182 451.72	182 382	70	4.5	64 $4d^2(^3F)5d\ ^4H$ + 33 $4d^2(^3F)5d\ ^4G$
182 782.89	182 767	16	1.5	91 $4d^2(^3F)5d\ ^4D$
182 924.12	183 012	−88	3.5	71 $4d^2(^3F)5d\ ^2F$ + 9 $4d^2(^3F)5d\ ^4D$ + 7 $4d^2(^3F)5d\ ^2G$
183 312.22	183 277	35	4.5	64 $4d^2(^3F)5d\ ^4G$ + 32 $4d^2(^3F)5d\ ^4H$
183 672.70	183 612	61	5.5	64 $4d^2(^3F)5d\ ^4H$ + 33 $4d^2(^3F)5d\ ^4G$
183 697.92	183 694	4	2.5	84 $4d^2(^3F)5d\ ^4D$ + 7 $4d^2(^3F)5d\ ^2F$
184 007.99	184 108	−100	0.5	48 $4d^2(^3F)5d\ ^2P$ + 25 $4d^2(^3F)5d\ ^4P$ + 14 $4d^2(^3F)5d\ ^4D$
184 547.29	184 527	20	5.5	64 $4d^2(^3F)5d\ ^4G$ + 35 $4d^2(^3F)5d\ ^4H$
184 987.76	185 000	−12	3.5	84 $4d^2(^3F)5d\ ^4D$ + 6 $4d^2(^3F)5d\ ^2G$ + 5 $4d^2(^3F)5d\ ^2F$
185 253.43	185 379	−126	1.5	44 $4d^2(^3F)5d\ ^4P$ + 38 $4d^2(^3F)5d\ ^2P$ + 8 $4d^2(^3P)5d\ ^4P$
185 283.50	185 262	22	6.5	99 $4d^2(^3F)5d\ ^4H$
185 412.03	185 440	−28	0.5	57 $4d^2(^3F)5d\ ^4P$ + 21 $4d^2(^3F)5d\ ^2P$ + 9 $4d^2(^3P)5d\ ^4P$
186 019.92	185 978	42	3.5	65 $4d^2(^3F)5d\ ^2G$ + 13 $4d^2(^3F)5d\ ^2F$ + 8 $4d^2(^1D)5d\ ^2G$
186 710.11	186 571	139	4.5	85 $4d^2(^3F)5d\ ^2H$ + 10 $4d^2(^1G)5d\ ^2H$
186 810.77	186 908	−97	1.5	38 $4d^2(^3F)5d\ ^4P$ + 31 $4d^2(^3F)5d\ ^2P$ + 15 $4d^2(^3F)5d\ ^2D$
186 931.08	186 976	−45	2.5	61 $4d^2(^3F)5d\ ^4P$ + 15 $4d^2(^3P)5d\ ^4P$ + 11 $4d^2(^3F)5d\ ^2D$
187 202.27	187 228	−26	1.5	74 $4d^2(^3F)5d\ ^4F$ + 11 $4d^2(^3F)5d\ ^2D$ + 8 $4d^2(^3F)5d\ ^2P$
187 237.70	187 192	46	4.5	79 $4d^2(^3F)5d\ ^2G$ + 10 $4d^2(^1D)5d\ ^2G$
187 688.42	187 725	−37	1.5	44 $4d^2(^3F)5d\ ^2D$ + 18 $4d^2(^3F)5d\ ^4F$ + 14 $4d^2(^1D)5d\ ^2D$
188 032.96	188 038	−5	2.5	82 $4d^2(^3F)5d\ ^4F$ + 5 $4d^2(^3F)5d\ ^2D$

Notes. [a] From Sugar & Musgrove (1988) and Cabeza et al. (1989). [b] This work. [c] Only the first three components that are larger than 5% are given.

Table A.5. continued.

E_{exp} [a]	E_{calc} [b]	ΔE	J	Leading components (in %) in LS coupling[c]
188 595.01	188 641	−46	2.5	53 $4d^2(^3F)5d\ ^2D$ + 17 $4d^2(^1D)5d\ ^2D$ + 12 $4d^2(^3F)5d\ ^4P$
188 709.85	188 615	95	5.5	86 $4d^2(^3F)5d\ ^2H$ + 10 $4d^2(^1G)5d\ ^2H$
188 979.01	188 982	−3	3.5	91 $4d^2(^3F)5d\ ^4F$
189 966.52	189 963	4	4.5	93 $4d^2(^3F)5d\ ^4F$
190 833.77	190 844	−10	1.5	96 $4d^2(^3F)6s\ ^4F$
191 339.64	191 333	7	2.5	77 $4d^2(^3F)6s\ ^4F$ + 19 $4d^2(^3F)6s\ ^2F$
191 540.13	191 524	16	1.5	59 $4d^2(^3P)5d\ ^2P$ + 35 $4d^2(^1D)5d\ ^2P$
191 755.47	191 757	−2	0.5	72 $4d^2(^1D)5d\ ^2S$ + 17 $4d^2(^3P)5d\ ^2P$
192 578.85	192 614	−35	3.5	88 $4d^2(^3F)6s\ ^4F$ + 8 $4d^2(^3F)6s\ ^2F$
192 624.98	192 633	−8	2.5	59 $4d^2(^1D)5d\ ^2F$ + 20 $4d^2(^3P)5d\ ^2F$ + 8 $4d^2(^3F)6s\ ^2F$
193 319.52	193 339	−19	3.5	55 $4d^2(^1D)5d\ ^2F$ + 10 $4d^2(^3P)5d\ ^4F$ + 10 $4d^2(^3P)5d\ ^2F$
193 379.15	193 435	−56	2.5	71 $4d^2(^3F)6s\ ^2F$ + 15 $4d^2(^3F)6s\ ^4F$ + 11 $4d^2(^1D)5d\ ^2F$
193 462.57	193 474	−12	0.5	42 $4d^2(^3P)5d\ ^2P$ + 27 $4d^2(^1D)5d\ ^2P$ + 20 $4d^2(^1D)5d\ ^2S$
193 779.78	193 718	62	4.5	38 $4d^2(^1D)5d\ ^2G$ + 31 $4d^2(^3P)5d\ ^4F$ + 19 $4d^2(^3F)6s\ ^4F$
193 815.29	193 805	10	1.5	92 $4d^2(^3P)5d\ ^4F$
194 100.67	194 059	42	3.5	49 $4d^2(^1D)5d\ ^2G$ + 20 $4d^2(^1D)5d\ ^2F$ + 9 $4d^2(^3P)5d\ ^4F$
194 235.12	194 244	−9	2.5	85 $4d^2(^3P)5d\ ^4F$ + 5 $4d^2(^3P)5d\ ^4D$
194 296.81	194 334	−37	4.5	78 $4d^2(^3F)6s\ ^4F$ + 15 $4d^2(^1D)5d\ ^2G$
194 970.47	194 952	18	3.5	63 $4d^2(^3P)5d\ ^4F$ + 10 $4d^2(^3P)5d\ ^2F$ + 8 $4d^2(^3P)5d\ ^4D$
195 307.98	195 298	10	1.5	72 $4d^2(^3P)5d\ ^4D$ + 15 $4d^2(^1D)5d\ ^2D$ + 6 $4d^2(^3F)5d\ ^2D$
195 454.02	195 423	31	3.5	85 $4d^2(^3F)6s\ ^2F$ + 7 $4d^2(^3F)6s\ ^4F$
195 672.25	195 653	19	0.5	89 $4d^2(^3P)5d\ ^4D$ + 6 $4d^2(^3P)5d\ ^2P$
195 740.65	195 722	19	2.5	81 $4d^2(^3P)5d\ ^4D$ + 5 $4d^2(^1D)5d\ ^2D$
196 151.58	196 092	60	2.5	44 $4d^2(^3P)5d\ ^2F$ + 36 $4d^2(^1G)5d\ ^2F$ + 11 $4d^2(^1D)5d\ ^2F$
196 179.49	196 187	−8	1.5	30 $4d^2(^3P)5d\ ^4P$ + 22 $4d^2(^1D)5d\ ^2D$ + 13 $4d^2(^3P)5d\ ^4D$
196 335.08	196 332	3	4.5	61 $4d^2(^3P)5d\ ^4F$ + 27 $4d^2(^1D)5d\ ^2G$ + 7 $4d^2(^1G)5d\ ^2G$
196 688.12	196 670	18	3.5	39 $4d^2(^3P)5d\ ^4D$ + 17 $4d^2(^1G)5d\ ^2F$ + 11 $4d^2(^3P)5d\ ^2F$
196 828.31	196 863	−35	3.5	38 $4d^2(^3P)5d\ ^4D$ + 33 $4d^2(^3P)5d\ ^2F$ + 12 $4d^2(^1G)5d\ ^2F$
196 953.22	196 943	10	0.5	56 $4d^2(^3P)5d\ ^4P$ + 17 $4d^2(^1D)5d\ ^2P$ + 14 $4d^2(^3P)5d\ ^2P$
197 119.54	197 108	12	2.5	55 $4d^2(^3P)5d\ ^4P$ + 18 $4d^2(^1D)5d\ ^2D$ + 15 $4d^2(^3F)5d\ ^4P$
197 258.73	197 292	−33	1.5	28 $4d^2(^3P)5d\ ^4P$ + 17 $4d^2(^3P)5d\ ^2D$ + 14 $4d^2(^1D)5d\ ^2D$
198 334.87	198 425	−90	2.5	26 $4d^2(^3P)5d\ ^2D$ + 21 $4d^2(^1G)5d\ ^2D$ + 18 $4d^2(^3P)5d\ ^4P$
198 712.48	198 686	26	0.5	39 $4d^2(^1D)5d\ ^2P$ + 28 $4d^2(^3P)5d\ ^4P$ + 17 $4d^2(^3P)5d\ ^2P$
199 069.41	199 165	−96	3.5	86 $4d^2(^1G)5d\ ^2G$ + 6 $4d^2(^3F)5d\ ^2G$ + 5 $4d^2(^1D)5d\ ^2G$
199 087.52	199 110	−22	1.5	24 $4d^2(^3P)5d\ ^2D$ + 20 $4d^2(^3P)5d\ ^4P$ + 19 $4d^2(^1D)5d\ ^2P$
199 229.00	199 252	−23	2.5	35 $4d^2(^1D)5d\ ^2D$ + 34 $4d^2(^3P)5d\ ^2D$ + 10 $4d^2(^1G)5d\ ^2D$
199 394.17	199 478	−84	4.5	73 $4d^2(^1G)5d\ ^2G$ + 12 $4d^2(^1G)5d\ ^2H$ + 7 $4d^2(^3F)5d\ ^2G$
199 722.50	199 711	12	5.5	98 $4d^2(^1G)5d\ ^2I$
200 086.20	200 048	38	6.5	99 $4d^2(^1G)5d\ ^2I$
200 189.54	200 189	1	1.5	23 $4d^2(^1D)5d\ ^2P$ + 18 $4d^2(^1D)5d\ ^2D$ + 18 $4d^2(^3P)5d\ ^2D$
201 009.39	200 995	14	4.5	76 $4d^2(^1G)5d\ ^2H$ + 9 $4d^2(^3F)5d\ ^2H$ + 8 $4d^2(^1G)5d\ ^2G$
201 022.59	200 980	43	5.5	86 $4d^2(^1G)5d\ ^2H$ + 11 $4d^2(^3F)5d\ ^2H$
201 355.10	201 306	49	2.5	71 $4d^2(^1D)6s\ ^2D$ + 26 $4d^2(^3P)6s\ ^4P$
201 545.32	201 488	57	1.5	79 $4d^2(^1D)6s\ ^2D$ + 9 $4d^2(^3P)6s\ ^4P$ + 8 $4d^2(^3P)6s\ ^2P$
202 114.64	202 120	−5	0.5	95 $4d^2(^3P)6s\ ^4P$
202 770.34	202 787	−17	1.5	86 $4d^2(^3P)6s\ ^4P$ + 8 $4d^2(^3P)6s\ ^2P$ + 5 $4d^2(^1D)6s\ ^2D$
203 894.00	203 890	4	0.5	96 $4d^2(^3P)6s\ ^2P$
204 269.40	204 276	−7	2.5	47 $4d^2(^3P)6s\ ^4P$ + 21 $4d^2(^1G)5d\ ^2F$ + 15 $4d^2(^1D)6s\ ^2D$
204 245.11	204 148	97	3.5	59 $4d^2(^1G)5d\ ^2F$ + 27 $4d^2(^3P)5d\ ^2F$ + 8 $4d^2(^1D)5d\ ^2F$
204 426.26	204 360	66	2.5	35 $4d^2(^1G)5d\ ^2F$ + 27 $4d^2(^3P)6s\ ^4P$ + 15 $4d^2(^3P)5d\ ^2F$
205 341.50	205 360	−18	1.5	82 $4d^2(^3P)6s\ ^2P$ + 12 $4d^2(^1D)6s\ ^2D$
206 861.16	206 904	−43	1.5	65 $4d^2(^1G)5d\ ^2D$ + 26 $4d^2(^3P)5d\ ^2D$
207 103.42	207 142	−39	2.5	60 $4d^2(^1G)5d\ ^2D$ + 29 $4d^2(^3P)5d\ ^2D$
207 561.80	207 554	8	4.5	99 $4d^2(^1G)6s\ ^2G$
207 567.86	207 556	12	3.5	98 $4d^2(^1G)6s\ ^2G$
221 465.60	221 414	52	1.5	94 $4d^2(^1S)5d\ ^2D$
221 491.80	221 541	−49	2.5	96 $4d^2(^1S)5d\ ^2D$
				Odd parity
109 415.25	109 428	−13	2.5	81 $4d^2(^3F)5p\ ^4G$ + 12 $4d^2(^3F)5p\ ^2F$
111 339.53	111 334	6	3.5	90 $4d^2(^3F)5p\ ^4G$ + 5 $4d^2(^3F)5p\ ^2F$
111 760.03	111 727	33	1.5	76 $4d^2(^3F)5p\ ^4F$ + 18 $4d^2(^3F)5p\ ^2D$
112 925.24	112 962	−37	2.5	71 $4d^2(^3F)5p\ ^4F$ + 12 $4d^2(^3F)5p\ ^2D$ + 7 $4d^2(^3F)5p\ ^4D$
113 443.02	113 424	19	4.5	92 $4d^2(^3F)5p\ ^4G$ + 6 $4d^2(^3F)5p\ ^4F$

Table A.5. continued.

E_{exp} [a]	E_{calc} [b]	ΔE	J	Leading components (in %) in LS coupling[c]
113 984.98	114 010	−25	2.5	39 $4d^2(^3F)5p\ ^2F$ + 21 $4d^2(^3F)5p\ ^4F$ + 16 $4d^2(^3F)5p\ ^4G$
114 624.49	114 561	63	3.5	90 $4d^2(^3F)5p\ ^4F$
114 708.24	114 756	−48	1.5	42 $4d^2(^3F)5p\ ^2D$ + 22 $4d^2(^3F)5p\ ^4F$ + 16 $4d^2(^3F)5p\ ^4D$
115 762.16	115 869	−107	3.5	62 $4d^2(^3F)5p\ ^2F$ + 23 $4d^2(^3F)5p\ ^4D$ + 6 $4d^2(^3F)5p\ ^4G$
115 789.36	115 729	60	0.5	79 $4d^2(^3F)5p\ ^4D$ + 17 $4d^2(^3P)5p\ ^4D$
115 881.12	115 816	65	5.5	99 $4d^2(^3F)5p\ ^4G$
115 961.91	115 897	65	4.5	84 $4d^2(^3F)5p\ ^4F$ + 7 $4d^2(^3F)5p\ ^2G$ + 7 $4d^2(^3F)5p\ ^4G$
116 583.82	116 641	−57	2.5	46 $4d^2(^3F)5p\ ^4D$ + 17 $4d^2(^3F)5p\ ^2F$ + 14 $4d^2(^3F)5p\ ^2D$
116 586.00	116 618	−32	1.5	61 $4d^2(^3F)5p\ ^4D$ + 16 $4d^2(^3P)5p\ ^4D$ + 12 $4d^2(^3F)5p\ ^2D$
117 604.08	117 752	−148	2.5	31 $4d^2(^3F)5p\ ^2D$ + 28 $4d^2(^3F)5p\ ^4D$ + 17 $4d^2(^3P)5p\ ^2D$
117 922.63	118 177	−255	0.5	92 $4d^2(^3P)5p\ ^2S$
118 080.17	118 097	−17	3.5	58 $4d^2(^3F)5p\ ^4D$ + 15 $4d^2(^3F)5p\ ^2F$ + 10 $4d^2(^3P)5p\ ^4D$
119 002.33	118 975	27	3.5	77 $4d^2(^3F)5p\ ^2G$ + 13 $4d^2(^1G)5p\ ^2G$
120 645.02	120 664	−19	4.5	72 $4d^2(^3F)5p\ ^2G$ + 15 $4d^2(^1G)5p\ ^2G$ + 11 $4d^2(^3F)5p\ ^4F$
120 823.46	120 749	74	1.5	69 $4d^2(^3P)5p\ ^4S$ + 22 $4d^2(^1D)5p\ ^2P$
122 419.26	122 399	20	0.5	80 $4d^2(^3P)5p\ ^4D$ + 17 $4d^2(^3F)5p\ ^4D$
122 808.84	122 887	−78	1.5	31 $4d^2(^1D)5p\ ^2P$ + 21 $4d^2(^3P)5p\ ^4S$ + 19 $4d^2(^3P)5p\ ^4D$
123 432.84	123 426	7	1.5	61 $4d^2(^3P)5p\ ^4D$ + 19 $4d^2(^1D)5p\ ^2P$ + 8 $4d^2(^3F)5p\ ^4D$
123 534.18	123 406	128	2.5	59 $4d^2(^1D)5p\ ^2F$ + 15 $4d^2(^3F)5p\ ^2F$ + 8 $4d^2(^3P)5p\ ^4D$
124 741.62	124 818	−76	0.5	82 $4d^2(^1D)5p\ ^2P$ + 12 $4d^2(^3P)5p\ ^4P$
124 789.75	124 723	67	2.5	70 $4d^2(^3P)5p\ ^4D$ + 14 $4d^2(^1D)5p\ ^2F$ + 9 $4d^2(^3F)5p\ ^4D$
124 947.54	124 828	120	3.5	43 $4d^2(^1D)5p\ ^2F$ + 20 $4d^2(^1G)5p\ ^2G$ + 16 $4d^2(^3P)5p\ ^4D$
126 243.19	126 330	−87	1.5	44 $4d^2(^1D)5p\ ^2D$ + 20 $4d^2(^1D)5p\ ^2P$ + 18 $4d^2(^3P)5p\ ^4P$
126 416.33	126 342	74	3.5	55 $4d^2(^3P)5p\ ^4D$ + 29 $4d^2(^1G)5p\ ^2G$ + 5 $4d^2(^3F)5p\ ^2G$
126 716.64	126 760	−43	2.5	53 $4d^2(^1D)5p\ ^2D$ + 29 $4d^2(^3P)5p\ ^4P$ + 6 $4d^2(^3F)5p\ ^2D$
126 760.46	126 707	53	0.5	83 $4d^2(^3P)5p\ ^4P$ + 9 $4d^2(^1D)5p\ ^2P$ + 6 $4d^2(^3P)5p\ ^2S$
126 999.09	126 897	102	4.5	70 $4d^2(^1G)5p\ ^2G$ + 19 $4d^2(^3F)5p\ ^2G$ + 10 $4d^2(^1G)5p\ ^2H$
127 181.20	127 129	52	1.5	77 $4d^2(^3P)5p\ ^4P$ + 18 $4d^2(^1D)5p\ ^2D$
127 728.82	127 634	95	3.5	33 $4d^2(^1G)5p\ ^2G$ + 32 $4d^2(^1D)5p\ ^2F$ + 17 $4d^2(^3P)5p\ ^4D$
128 897.78	128 862	36	2.5	64 $4d^2(^3P)5p\ ^4P$ + 32 $4d^2(^1D)5p\ ^2D$
130 149.35	129 987	162	4.5	87 $4d^2(^1G)5p\ ^2H$ + 12 $4d^2(^1G)5p\ ^2G$
131 699.83	131 641	59	1.5	65 $4d^2(^3P)5p\ ^2D$ + 13 $4d^2(^3P)5p\ ^2P$ + 13 $4d^2(^3F)5p\ ^2D$
132 012.37	131 849	163	5.5	99 $4d^2(^1G)5p\ ^2H$
132 219.07	132 241	−22	2.5	70 $4d^2(^3P)5p\ ^2D$ + 20 $4d^2(^3F)5p\ ^2D$
133 362.00	133 350	12	0.5	92 $4d^2(^3P)5p\ ^2P$
134 242.50	134 223	20	1.5	79 $4d^2(^3P)5p\ ^2P$ + 9 $4d^2(^3P)5p\ ^2D$
134 951.06	135 198	−247	3.5	90 $4d^2(^1G)5p\ ^2F$
136 324.44	136 602	−278	2.5	94 $4d^2(^1G)5p\ ^2F$
150 069.22	150 096	−27	0.5	92 $4d^2(^1S)5p\ ^2P$
152 757.31	152 729	28	1.5	95 $4d^2(^1S)5p\ ^2P$

Table A.6. Comparison between available experimental and calculated energy levels in Mo V. Energies are given in cm^{-1}.

E_{exp} [a]	E_{calc} [b]	ΔE	J	Leading components (in %) in LS coupling[c]
				Even parity
0.00	12	−12	2	97 $4d^2\ ^3F$
1577.17	1577	0	3	99 $4d^2\ ^3F$
3357.08	3345	12	4	98 $4d^2\ ^3F$
10 190.11	10 186	4	2	76 $4d^2\ ^1D$ + 21 $4d^2\ ^3P$
11 161.31	11 149	12	0	98 $4d^2\ ^3P$
11 806.93	11 808	−1	1	99 $4d^2\ ^3P$
13 408.30	13 423	−15	2	78 $4d^2\ ^3P$ + 21 $4d^2\ ^1D$
16 353.36	16 353	0	4	98 $4d^2\ ^1G$
37 737.83	37 738	0	0	98 $4d^2\ ^1S$
92 380.54	92 375	5	1	99 4d5s ^3D
93 111.40	93 118	−7	2	95 4d5s ^3D
94 835.44	94 834	1	3	99 4d5s ^3D
99 380.40	99 380	0	2	95 4d5s ^1D
199 050.87	199 051	0	0	96 $5s^2\ ^1S$
232 561.12	232 576	−15	3	79 4d5d ^1F + 11 4d5d ^3G + 8 4d5d ^3D
233 190.31	233 194	−4	1	81 4d5d ^3D + 18 4d5d ^1P
234 252.45	234 252	0	2	97 4d5d ^3D
234 490.48	234 468	22	3	82 4d5d ^3G + 10 4d5d ^3D + 5 4d5d ^1F
235 496.01	235 472	24	4	97 4d5d ^3G
235 634.96	235 640	−5	3	80 4d5d ^3D + 14 4d5d ^1F + 5 4d5d ^3G
236 002.02	236 033	−31	1	73 4d5d ^1P + 18 4d5d ^3D + 7 4d5d ^3S
237 204.53	237 183	22	5	99 4d5d ^3G
237 759.53	237 755	5	2	93 4d5d ^3F + 5 4d5d ^1D
239 068.95	239 071	−2	3	96 4d5d ^3F
239 188.82	239 203	−14	1	88 4d5d ^3S + 8 4d5d ^1P
240 109.61	240 111	−1	4	96 4d5d ^3F
241 964.75	241 971	−6	2	70 4d5d ^1D + 23 4d5d ^3P
242 161.93	242 171	−9	0	96 4d5d ^3P
242 971.44	242 962	9	1	95 4d5d ^3P
243 954.32	243 952	2	2	75 4d5d ^3P + 23 4d5d ^1D
244 170.15	244 167	3	4	96 4d5d ^1G
251 017.96	251 018	0	0	94 4d5d ^1S
254 125.95	254 125	1	1	100 4d6s ^3D
254 464.98	254 466	−1	2	77 4d6s ^3D + 23 4d6s ^1D
256 676.48	256 677	−1	3	100 4d6s ^3D
257 442.81	257 442	1	2	77 4d6s ^1D + 23 4d6s ^3D
314 344.75	314 213	131	0	76 $5p^2\ ^3P$ + 18 4d6d ^3P
320 344.53	320 431	−86	2	64 4d6d ^1D + 11 $5p^2\ ^1D$ + 8 4d6d ^3P
320 917.27	321 522	−605	1	68 4d6d ^3P + 26 $5p^2\ ^3P$
323 777.46	323 661	116	2	50 $5p^2\ ^3P$ + 32 4d6d ^3P + 8 $5p^2\ ^1D$
327 070.61	327 063	8	5	37 4d5g ^1H + 37 4d5g ^3H + 25 4d5g ^3G
327 141.68	327 129	13	4	74 4d5g ^3H + 16 4d5g ^3G + 10 4d5g ^1G
327 386.30	327 370	16	3	63 4d5g ^3G + 22 4d5g ^1F + 15 4d5g ^3F
327 436.40	327 436	0	4	37 4d5g ^3F + 32 4d5g ^3G + 30 4d5g ^1G
327 859.16	327 879	−20	5	70 4d5g ^3I + 15 4d5g ^3H + 14 4d5g ^1H
327 995.37	328 035	−40	6	42 4d5g ^3I + 32 4d5g ^3H + 26 4d5g ^1I
328 234.03	328 216	18	3	47 4d5g ^3D + 30 4d5g ^3F + 22 4d5g ^1F
328 265.06	328 263	2	2	54 4d5g ^3F + 26 4d5g ^1D + 19 4d5g ^3D
329 713.88	329 715	−1	5	68 4d5g ^3G + 26 4d5g ^1H
329 795.97	329 799	−3	4	39 4d5g ^3G + 34 4d5g ^1G + 24 4d5g ^3H
329 810.15	329 812	−2	5	44 4d5g ^3H + 26 4d5g ^3I + 23 4d5g ^1H
329 897.53	329 906	−8	6	68 4d5g ^3H + 24 4d5g ^3I + 8 4d5g ^1I
330 052.53	330 030	23	3	37 4d5g ^1F + 37 4d5g ^3G + 26 4d5g ^3F
330 100.52	330 090	11	4	61 4d5g ^3F + 26 4d5g ^1G + 13 4d5g ^3G
330 656.07	330 687	−31	7	100 4d5g ^3I
330 667.37	330 642	25	3	52 4d5g ^3D + 29 4d5g ^3F + 19 4d5g ^1F
330 699.70	330 689	11	2	46 4d5g ^3F + 28 4d5g ^3D + 25 4d5g ^1D
330 878.23	330 943	−65	6	65 4d5g ^1I + 34 4d5g ^3I
331 233.74	331 189	45	1	99 4d5g ^3D
331 263.46	331 262	1	2	51 4d5g ^3D + 47 4d5g ^1D
346 764.00	346 827	−63	1	98 5s5d ^3D

Notes. [a] From Reader & Tauheed (2015). [b] This work. [c] Only the first three components that are larger than 5% are given.

Table A.6. continued.

E_{exp} [a]	E_{calc} [b]	ΔE	J	Leading components (in %) in LS coupling[c]
347 006.81	347 023	−16	2	98 5s5d ^{3}D
347 408.70	347 331	78	3	98 5s5d ^{3}D
349 643.40	349 647	−4	0	85 5p^2 ^{1}S + 7 4d6d ^{1}S
368 808.38	368 808	0	1	100 5s6s ^{3}S
				Odd parity
146 976.75	146 976	1	2	53 4d5p ^{1}D + 42 4d5p ^{3}F
148 948.66	148 841	108	1	93 4d5p ^{3}D
150 345.79	150 449	−103	2	48 4d5p ^{3}D + 27 4d5p ^{1}D + 18 4d5p ^{3}F
151 195.14	151 178	17	3	69 4d5p ^{3}F + 28 4d5p ^{3}D
151 213.20	151 163	50	2	45 4d5p ^{3}D + 39 4d5p ^{3}F + 15 4d5p ^{1}D
153 039.67	153 077	−37	3	67 4d5p ^{3}D + 30 4d5p ^{3}F
155 032.33	155 054	−22	4	99 4d5p ^{3}F
156 616.49	156 549	67	1	84 4d5p ^{3}P + 11 4d5p ^{1}P
157 059.18	157 034	25	0	99 4d5p ^{3}P
157 851.46	157 928	−77	2	92 4d5p ^{3}P
159 856.69	159 923	−66	3	94 4d5p ^{1}F
162 257.12	162 221	36	1	83 4d5p ^{1}P + 13 4d5p ^{3}P
237 482.33	237 668	−186	4	83 4d4f ^{1}G + 7 4d4f ^{3}F
239 392.83	239 263	130	2	82 4d4f ^{3}F + 13 4d4f ^{1}D
239 949.69	240 199	−249	4	80 4d4f ^{3}H + 13 4d4f ^{3}F
240 004.70	239 937	68	3	90 4d4f ^{3}F
240 725.04	241 156	−431	5	95 4d4f ^{3}H
240 878.05	241 046	−168	4	72 4d4f ^{3}F + 12 4d4f ^{3}H + 11 4d4f ^{1}G
241 752.33	242 135	−383	2	79 4d4f ^{1}D + 12 4d4f ^{3}F
241 972.61	242 613	−640	6	98 4d4f ^{3}H
243 408.59	242 726	683	3	82 4d4f ^{3}G + 8 4p^{5}4d^3(^{2}H)^{3}G
244 626.80	244 102	525	4	83 4d4f ^{3}G + 7 4p^{5}4d^3(^{2}H)^{3}G
245 600.22	245 199	401	5	87 4d4f ^{3}G + 7 4p^{5}4d^3(^{2}H)^{3}G
246 619.40	246 889	−270	0	67 5s5p ^{3}P + 31 4d4f ^{3}P
246 799.61	246 586	214	1	54 4d4f ^{3}D + 22 4d4f ^{3}P + 14 5s5p ^{3}P
247 090.71	246 813	278	2	59 4d4f ^{3}D + 27 4d4f ^{3}P
247 687.61	247 406	282	3	83 4d4f ^{3}D + 6 4d4f ^{1}F
247 932.56	247 852	81	1	36 5s5p ^{3}P + 34 4d4f ^{3}D + 24 4d4f ^{3}P
248 745.05	248 576	169	2	47 4d4f ^{3}P + 31 4d4f ^{3}D + 15 5s5p ^{3}P
250 990.91	250 913	78	3	85 4d4f ^{1}F + 6 4d4f ^{3}D
252 463.44	252 209	254	0	63 4d4f ^{3}P + 33 5s5p ^{3}P
252 648.40	252 507	141	1	48 4d4f ^{3}P + 47 5s5p ^{3}P
254 209.83	254 298	−88	2	79 5s5p ^{3}P + 18 4d4f ^{3}P
255 941.37	255 888	53	1	80 4d4f ^{1}P + 14 5s5p ^{1}P
259 254.51	259 880	−625	5	92 4d4f ^{1}H
275 024.25	274 831	193	1	46 5s5p ^{1}P + 31 4d6p ^{1}P + 12 4d6p ^{3}D
276 470.33	276 478	−8	2	45 4d6p ^{3}F + 41 4d6p ^{1}D + 12 4d6p ^{3}D
277 187.91	277 191	−3	1	85 4d6p ^{3}D + 11 5s5p ^{1}P
278 004.86	277 960	45	2	60 4d6p ^{3}D + 35 4d6p ^{3}F
278 999.30	278 971	28	3	68 4d6p ^{3}F + 16 4d6p ^{3}D + 16 4d6p ^{1}F
279 060.06	279 214	−154	2	44 4d6p ^{1}D + 27 4d6p ^{3}D + 18 4d6p ^{3}F
279 478.11	279 478	0	3	65 4d6p ^{3}D + 27 4d6p ^{3}F + 7 4d6p ^{1}F
280 277.20	280 478	−201	4	38 4p^{5}4d^3(^{4}P)^{5}D + 33 4p^{5}4d^3(^{4}F)^{5}D + 26 4p^{5}4d^3(^{4}F)^{5}F
280 279.09	280 081	198	0	99 4d6p ^{3}P
280 505.47	280 414	91	1	92 4d6p ^{3}P
281 268.15	281 479	−211	4	100 4d6p ^{3}F
281 996.44	281 709	287	3	75 4d6p ^{1}F + 19 4d6p ^{3}D
282 057.02	282 025	32	2	88 4d6p ^{3}P + 10 4d6p ^{1}D
285 619.22	286 160	−541	1	65 4d6p ^{1}P + 19 5s5p ^{1}P + 6 4d4f ^{1}P
287 427.80	287 135	293	4	52 4p^{5}4d^3(^{4}F)^{5}F + 19 4p^{5}4d^3(^{4}P)^{5}D + 17 4p^{5}4d^3(^{4}F)^{5}G
287 471.40	287 899	−428	3	51 4p^{5}4d^3(^{4}F)^{5}F + 15 4p^{5}4d^3(^{4}P)^{5}D + 13 4p^{5}4d^3(^{4}F)^{5}G
287 818.70	287 881	−62	1	76 4p^{5}4d^3(^{4}F)^{5}F + 6 4p^{5}4d^3(^{4}F)^{5}D + 5 4p^{5}4d^3(^{4}F)^{3}D
287 997.70	287 965	33	2	57 4p^{5}4d^3(^{4}F)^{5}F + 10 4p^{5}4d^3(^{4}F)^{5}D + 9 4p^{5}4d^3(^{4}P)^{5}D
294 230.46	294 553	−323	2	46 4p^{5}4d^3(^{2}G)^{3}F + 20 4p^{5}4d^3(^{4}F)^{3}F + 9 4p^{5}4d^3(^{4}F)^{5}G
294 925.20	294 691	234	5	66 4p^{5}4d^3(^{4}F)^{5}G + 15 4p^{5}4d^3(^{4}F)^{5}F + 10 4p^{5}4d^3(^{4}F)^{3}G
296 151.14	296 102	49	4	36 4p^{5}4d^3(^{4}F)^{5}G + 17 4p^{5}4d^3(^{2}H)^{3}G + 16 4p^{5}4d^3(^{4}F)^{3}G
296 191.62	296 489	−297	3	31 4p^{5}4d^3(^{2}G)^{3}F + 19 4p^{5}4d^3(^{2}H)^{3}G + 10 4p^{5}4d^3(^{4}F)^{3}F
297 369.77	297 386	−16	3	32 4p^{5}4d^3(^{4}F)^{5}G + 11 4p^{5}4d^3(^{4}F)^{3}G

Table A.6. continued.

E_{exp} [a]	E_{calc} [b]	ΔE	J	Leading components (in %) in LS coupling[c]
297 428.25	297 454	−26	2	41 $4p^5 4d^3(^2P)^3P$ + 13 $4p^5 4d^3(^2D)^3P$ + 12 $4p^5 4d^3(^2D)^3D$
298 928.26	298 886	42	4	29 $4p^5 4d^3(^2G)^3F$ + 14 $4p^5 4d^3(^4F)^5G$ + 12 $4p^5 4d^3(^4F)^3F$
299 310.36	299 268	42	1	34 $4p^5 4d^3(^2P)^3P$ + 20 $4p^5 4d^3(^2D)^3P$ + 10 $4p^5 4d^3(^2D)^3D$
299 916.96	299 865	52	3	32 $4p^5 4d^3(^2D)^3D$ + 13 $4p^5 4d^3(^2P)^3D$ + 12 $4p^5 4d^3(^4F)^3D$
301 540.26	300 802	738	5	27 $4p^5 4d^3(^2F)^3G$ + 21 $4p^5 4d^3(^2H)^3G$ + 19 $4p^5 4d^3(^2G)^3G$
301 775.31	301 725	50	4	19 $4p^5 4d^3(^4F)^5G$ + 14 $4p^5 4d^3(^2G)^1G$ + 11 $4p^5 4d^3(^2H)^1G$
301 935.30	301 818	117	0	41 $4p^5 4d^3(^2P)^3P$ + 27 $4p^5 4d^3(^2D)^3P$ + 14 $4p^5 4d^3(^2D)^3P$
302 869.95	302 640	230	2	20 $4p^5 4d^3(^2D)^3D$ + 18 $4p^5 4d^3(^2P)^3P$ + 15 $4p^5 4d^3(^2P)^3D$
303 813.31	303 776	37	1	24 $4p^5 4d^3(^2D)^3D$ + 14 $4p^5 4d^3(^2P)^3P$ + 13 $4p^5 4d^3(^2F)^3D$
303 955.54	303 688	268	3	36 $4p^5 4d^3(^4F)^5G$ + 20 $4d5f\ ^3G$ + 12 $4p^5 4d^3(^2H)^3G$
304 727.38	304 885	−158	3	38 $4p^5 4d^3(^2P)^3D$ + 27 $4d5f\ ^3D$ + 7 $4p^5 4d^3(^2F)^3D$
304 828.89	304 592	237	6	82 $4p^5 4d^3(^2G)^3H$ + 9 $4p^5 4d^3(^2H)^3I$
304 831.60	304 532	300	2	73 $4p^5 4d^3(^4F)^5G$ + 11 $4p^5 4d^3(^2G)^3F$
306 037.34	306 133	−96	4	25 $4d5f\ ^3G$ + 13 $4d5f\ ^1G$ + 12 $4p^5 4d^3(^2G)^1G$
306 992.33	306 846	146	5	49 $4p^5 4d^3(^2G)^3H$ + 18 $4d5f\ ^3G$ + 8 $4d5f\ ^3H$
307 588.25	307 218	370	4	55 $4p^5 4d^3(^2D)^3F$ + 21 $4p^5 4d^3(^2F)^3F$
307 863.79	307 636	228	2	35 $4d5f\ ^3D$ + 22 $4p^5 4d^3(^2P)^3D$ + 13 $4p^5 4d^3(^2F)^3D$
308 939.76	308 963	−23	3	24 $4d5f\ ^1F$ + 17 $4p^5 4d^3(^2D)^3F$ + 13 $4p^5 4d^3(^2D)^1F$
310 475.83	310 307	169	1	32 $4d5f\ ^3D$ + 21 $4p^5 4d^3(^2P)^3D$ + 8 $4p^5 4d^3(^2F)^3D$
310 668.20	310 405	263	3	22 $4d5f\ ^3G$ + 20 $4d5f\ ^3F$ + 16 $4p^5 4d^3(^2G)^3G$
311 070.16	311 095	−25	4	27 $4d5f\ ^3H$ + 22 $4d5f\ ^1G$ + 8 $4p^5 4d^3(^2G)^3G$
311 351.67	311 402	−50	2	52 $4d5f\ ^1D$ + 11 $4d5f\ ^3F$ + 6 $4d5f\ ^3P$
311 959.68	311 636	324	5	36 $4d5f\ ^3G$ + 26 $4p^5 4d^3(^2G)^3G$ + 16 $4p^5 4d^3(^2G)^1H$
312 298.30	312 238	60	3	73 $4p^5 4d^3(^4P)^5P$ + 10 $4p^5 4d^3(^4F)^5D$ + 5 $4p^5 4d^3(^4P)^5D$
312 368.08	312 698	−330	2	17 $4d5f\ ^3F$ + 15 $4p^5 4d^3(^4P)^5P$ + 14 $4d5f\ ^3P$
313 207.16	313 434	−227	2	39 $4d5f\ ^3F$ + 25 $4d5f\ ^1D$ + 9 $4p^5 4d^3(^2D)^3F$
313 772.78	314 068	−295	3	36 $4d5f\ ^3F$ + 16 $4p^5 4d^3(^2F)^3F$ + 10 $4p^5 4d^3(^2D)^3F$
313 919.45	313 743	176	4	61 $4d5f\ ^3F$ + 7 $4p^5 4d^3(^2F)^3F$ + 5 $4p^5 4d^3(^4F)^5D$
314 526.51	314 494	33	4	52 $4d5f\ ^3H$ + 15 $4d5f\ ^3G$ + 12 $4p^5 4d^3(^2G)^3G$
315 617.49	315 048	569	5	55 $4p^5 4d^3(^2H)^3I$ + 22 $4p^5 4d^3(^2H)^3H$ + 8 $4p^5 4d^3(^2G)^3H$
315 691.14	315 526	165	3	24 $4d5f\ ^1F$ + 21 $4d5f\ ^3F$ + 15 $4d5f\ ^3G$
316 289.19	316 628	−339	4	46 $4d5f\ ^1G$ + 10 $4p^5 4d^3(^2G)^1G$ + 8 $4p^5 4d^3(^2H)^3H$
316 463.94	316 224	240	5	79 $4d5f\ ^3H$ + 8 $4p^5 4d^3(^2H)^3I$
316 539.85	316 044	496	1	39 $4d5f\ ^3P$ + 24 $4p^5 4d^3(^4P)^5P$ + 10 $4p^5 4d^3(^2P)^3S$
316 643.63	316 831	−187	6	74 $4d5f\ ^3H$ + 12 $4p^5 4d^3(^2H)^3H$ + 8 $4p^5 4d^3(^2H)^1I$
316 690.26	316 404	286	2	39 $4d5f\ ^3P$ + 9 $4p^5 4d^3(^4P)^5P$ + 9 $4p^5 4d^3(^4P)^5D$
319 064.90	319 214	−149	3	31 $4p^5 4d^3(^4F)^5D$ + 29 $4p^5 4d^3(^4P)^5D$ + 10 $4p^5 4d^3(^4P)^5P$
319 484.00	319 614	−130	0	49 $4p^5 4d^3(^4P)^5D$ + 17 $4p^5 4d^3(^4F)^5D$ + 13 $4p^5 4d^3(^2P)^1S$
319 648.03	319 104	544	5	48 $4d5f\ ^1H$ + 18 $4p^5 4d^3(^2G)^3H$ + 8 $4p^5 4d^3(^2F)^3G$
319 779.02	320 146	−367	2	20 $4p^5 4d^3(^4P)^5P$ + 17 $4p^5 4d^3(^4P)^3D$ + 16 $4p^5 4d^3(^4P)^5D$
320 795.31	320 432	363	3	28 $4p^5 4d^3(^4F)^3G$ + 12 $4p^5 4d^3(^2G)^3G$ + 11 $4d5f\ ^1F$
321 070.92	320 838	233	4	41 $4p^5 4d^3(^2G)^3H$ + 12 $4p^5 4d^3(^4F)^3G$ + 8 $4d5f\ ^3H$
323 010.78	323 038	−27	3	41 $4d5f\ ^3D$ + 18 $4p^5 4d^3(^2P)^3D$ + 7 $4d5f\ ^1F$
323 076.60	323 184	−107	1	17 $4p^5 4d^3(^4P)^3D$ + 14 $4d5f\ ^1P$ + 14 $4d5f\ ^3D$
323 151.83	322 790	362	4	22 $4p^5 4d^3(^2D)^3F$ + 16 $4p^5 4d^3(^2F)^3G$ + 14 $4p^5 4d^3(^4F)^3G$
325 021.00	326 124	−1103	3	18 $4p^5 4d^3(^2D)^3F$ + 15 $4p^5 4d^3(^2D)^1F$ + 14 $4p^5 4d^3(^2F)^3F$
325 451.40	325 785	−334	2	24 $4p^5 4d^3(^4P)^5P$ + 19 $4d5f\ ^3D$ + 8 $4p^5 4d^3(^4P)^5D$
325 482.90	325 966	−483	4	30 $4p^5 4d^3(^2D)^3F$ + 20 $4p^5 4d^3(^4F)^3G$ + 10 $4p^5 4d^3(^2F)^3F$
325 636.30	325 093	543	5	36 $4p^5 4d^3(^4F)^3G$ + 27 $4p^5 4d^3(^2F)^3G$ + 11 $4p^5 4d^3(^2H)^3H$
327 058.60	327 568	−509	2	17 $4p^5 4d^3(^4P)^3P$ + 10 $4p^5 4d^3(^2D)^3P$ + 9 $4p^5 4d^3(^2F)^1D$
327 147.00	327 349	−202	0	24 $4p^5 4d^3(^4P)^3P$ + 23 $4d5f\ ^3P$
329 436.00	329 202	234	2	12 $4p^5 4d^3(^4P)^5P$ + 12 $4p^5 4d^3(^2F)^3F$ + 11 $4p^5 4d^3(^2P)^3D$
329 481.50	329 232	250	4	62 $4p^5 4d^3(^2H)^3H$ + 10 $4p^5 4d^3(^2G)^1G$ + 9 $4p^5 4d^3(^4F)^3G$
329 793.78	330 022	228	5	18 $4p^5 4d^3(^4F)^3G$ + 12 $4p^5 4d^3(^2G)^3G$ + 12 $4p^5 4d^3(^2H)^3H$
330 042.70	330 219	−176	3	25 $4p^5 4d^3(^4P)^3D$ + 15 $4p^5 4d^3(^2F)^3D$ + 10 $4p^5 4d^3(^2D)^3F$
331 039.00	330 940	99	5	45 $4p^5 4d^3(^2H)^3H$ + 12 $4p^5 4d^3(^2F)^3G$ + 9 $4p^5 4d^3(^2H)^3I$
331 241.30	331 773	−532	1	48 $4p^5 4d^3(^2P)^3D$ + 16 $4d5f\ ^3D$ + 7 $4p^5 4d^3(^2D)^3D$
333 683.90	333 950	−266	4	24 $4p^5 4d^3(^2G)^3G$ + 23 $4p^5 4d^3(^2F)^1G$ + 20 $4p^5 4d^3(^2F)^3G$
335 185.90	335 792	−605	3	18 $4p^5 4d^3(^2D)^3F$ + 12 $4p^5 4d^3(^2F)^3G$ + 12 $4p^5 4d^3(^2D)^1F$
335 518.50	335 117	402	0	45 $4p^5 4d^3(^2P)^3P$ + 37 $4p^5 4d^3(^2D)^3P$ + 13 $4p^5 4d^3(^2P)^1S$
339 075.10	338 926	149	2	24 $4p^5 4d^3(^2D)^3F$ + 15 $4p^5 4d^3(^2D)^3P$ + 11 $4p^5 4d^3(^2P)^1D$
339 315.90	340 261	−945	3	31 $4p^5 4d^3(^2F)^3G$ + 17 $4p^5 4d^3(^2G)^3G$ + 10 $4d5f\ ^3G$
339 672.90	339 529	144	5	39 $4p^5 4d^3(^2G)^1H$ + 20 $4p^5 4d^3(^2G)^3G$ + 9 $4p^5 4d^3(^2G)^3H$
341 107.60	341 139	−31	2	44 $4p^5 4d^3(^2D)^3P$ + 15 $4p^5 4d^3(^2P)^3P$ + 13 $4p^5 4d^3(^2P)^1D$

Table A.6. continued.

E_{exp} [a]	E_{calc} [b]	ΔE	J	Leading components (in %) in LS coupling[c]
343 064.20	343 404	−340	4	29 $4p^5 4d^3(^2F)^1G$ + 16 $4p^5 4d^3(^2D)^3F$ + 12 $4p^5 4d^3(^2F)^3G$
345 339.60	346 017	−677	3	28 4d6f ^3G + 16 $4p^5 4d^3(^2H)^3G$ + 7 4d5f ^3G
347 173.53	347 194	−20	2	91 5s4f ^3F + 5 $4p^5 4d^2 5s(^1G)^3F$
347 303.47	347 354	−51	3	90 5s4f ^3F
347 509.30	347 154	355	4	27 4d6f ^3G + 11 $4p^5 4d^3(^2H)^3G$ + 5 $4p^5 4d^3(^2D)^3F$
347 675.00	347 626	49	4	84 5s4f ^3F
349 517.60	349 398	120	5	46 4d6f ^3G + 14 $4p^5 4d^3(^2H)^3G$ + 10 $4p^5 4d^3(^4F)^3G$
349 710.90	349 517	194	3	20 $4p^5 4d^3(^2D)^3F$ + 17 $4p^5 4d^3(^2F)^3F$ + 11 $4p^5 4d^3(^2D)^3F$
349 902.70	349 664	239	4	14 $4p^5 4d^3(^2F)^3F$ + 14 $4p^5 4d^3(^2F)^3G$ + 14 $4p^5 4d^3(^2F)^1G$
350 465.80	350 509	−43	2	54 4d6f ^1D + 23 4d6f ^3F + 5 $4p^5 4d^3(^2D)^1D$
351 332.70	351 241	92	2	20 4d6f ^3F + 15 4d6f ^3D + 5 $4p^5 4d^3(^2D)^3F$
351 932.60	352 021	−88	3	28 5s4f ^1F + 25 4d6f ^1F + 17 4d6f ^3D
353 002.30	352 410	592	1	50 4d6f ^3D + 21 4d6f ^3P + 6 4d6f ^1P
353 268.90	353 248	21	3	39 5s4f ^1F + 20 4d6f ^3F + 18 4d6f ^3D
353 671.83	353 284	388	2	31 4d6f ^3D + 23 4d6f ^3P + 13 4d6f ^3F
354 169.92	353 899	271	3	47 4d6f ^3F + 29 4d6f ^3D
354 247.00	354 112	135	4	46 4d6f ^3F + 37 4d6f ^3H
354 542.54	354 315	227	5	53 4d6f ^3H + 25 4d6f ^1H + 8 4d6f ^3G
354 582.30	354 480	102	2	30 4d6f ^3F + 14 4d6f ^3P + 11 $4p^5 4d^3(^2F)^3F$
354 959.83	354 943	17	4	55 4d6f ^1G + 24 4d6f ^3F + 14 4d6f ^3H
355 095.60	354 717	379	0	82 4d6f ^3P + 11 $4p^5 4d^3(^4P)^3P$
356 149.65	356 068	82	3	54 4d6f ^1F + 19 5s4f ^1F + 6 4d6f ^3D
356 387.52	355 899	489	5	43 4d6f ^3H + 35 4d6f ^1H + 14 $4p^5 4d^3(^2H)^1H$
358 278.19	358 202	76	1	84 4d6f ^1P
359 499.00	359 424	75	3	28 $4p^5 4d^3(^2D)^3D$ + 21 $4p^5 4d^3(^2D)^1F$ + 16 $4p^5 4d^3(^2D)^3D$
363 720.60	366 218	−2497	3	43 4d6f ^3G + 22 4d7f ^3G + 12 $4p^5 4d^3(^2H)^3G$
365 766.80	368 161	−2394	4	37 4d6f ^3G + 30 4d7f ^3G + 13 $4p^5 4d^3(^2H)^3G$
366 751.60	366 516	236	2	43 $4p^5 4d^3(^2D)^3D$ + 24 $4p^5 4d^3(^2D)^3D$ + 15 $4p^5 4d^3(^2F)^3D$
366 892.60	369 103	−2210	5	24 4d6f ^3G + 22 4d7f ^3G + 9 $4p^5 4d^3(^2H)^3G$
367 517.40	367 806	−289	2	36 $4p^5 4d^3(^2D)^1D$ + 35 $4p^5 4d^3(^2D)^1D$ + 8 $4p^5 4d^3(^2D)^3F$
368 492.20	367 727	765	3	23 $4p^5 4d^3(^2F)^1F$ + 19 $4p^5 4d^3(^2D)^1F$ + 17 $4p^5 4d^3(^2D)^3D$
371 078.10	371 292	−214	1	40 4d7f ^3D + 13 4d6f ^3D + 10 $4p^5 4d^3(^2D)^3D$
371 811.60	372 022	−210	2	25 4d7f ^1D + 22 4d7f ^3D + 16 4d7f ^3F
372 444.90	373 055	−610	5	38 4d7f ^1H + 16 $4p^5 4d^3(^2H)^1H$ + 16 4d7f ^3G
373 453.50	373 046	408	3	40 4d7f ^3D + 22 4d7f ^1F + 6 4d7f ^3F
375 034.50	374 431	604	2	50 4d7f ^3F + 13 4d7f ^3P + 7 $4p^5 4d^3(^4F)^3F$
375 165.80	374 710	456	1	57 4d7f ^3P + 9 $4p^5 4d^3(^4P)^3P$ + 6 4d6f ^3P
375 355.10	374 621	734	3	67 4d7f ^3F + 9 $4p^5 4d^3(^4F)^3F$ + 6 4d7f ^1F
377 569.20	375 812	1757	4	64 4d7f ^3H + 25 4d7f ^3F
377 999.30	376 923	1076	4	57 4d7f ^1G + 21 4d7f ^3H + 14 4d7f ^3F
378 160.50	377 083	1077	5	95 4d7f ^3H
381 105.40	381 993	−888	3	64 4d7f ^3G + 11 4d8f ^3G + 7 $4p^5 4d^3(^2H)^3G$
382 612.30	383 691	−1079	4	60 4d7f ^3G + 16 4d8f ^3G + 8 $4p^5 4d^3(^2H)^3G$
383 279.50	384 509	−1230	5	38 4d7f ^3G + 17 4d7f ^1H + 12 4d8f ^3G
383 895.40	383 758	137	1	41 4d7f ^3D + 13 4d8f ^3D + 6 $4p^5 4d^3(^2F)^3D$
384 886.50	385 093	−206	3	67 $4p^5 4d^2 5s(^3F)^5D$ + 23 $4p^5 4d^2 5s(^3P)^5D$ + 5 $4p^5 4d^2 5s(^3F)^5F$
385 431.20	385 190	241	2	28 4d7f ^3D + 19 4d8f ^3D + 7 $4p^5 4d^3(^2F)^3D$
385 599.50	387 275	−1675	5	28 4d8f ^1H + 20 4d7f ^1H + 10 $4p^5 4d^3(^2H)^1H$
386 020.80	386 175	−154	2	17 4d8f ^1D + 15 4d8f ^3F + 9 $4p^5 4d^3(^4F)^3F$
386 919.80	387 815	−895	1	36 4d8f ^3P + 21 4d7f ^3P + 10 $4p^5 4d^3(^4P)^3P$
387 095.30	387 690	−595	2	19 4d8f ^3P + 17 4d8f ^3F + 10 $4p^5 4d^3(^4F)^3F$
388 410.00	387 869	541	3	39 4d8f ^3F + 17 $4p^5 4d^3(^4F)^3F$ + 15 4d7f ^3F
389 382.80	389 203	180	4	52 4d8f ^3F + 12 4d8f ^1G + 11 $4p^5 4d^3(^4F)^3F$
389 461.40	389 065	396	3	37 4d8f ^1F + 9 4d7f ^1F + 8 4d8f ^3D
389 545.00	389 724	−179	2	33 4d8f ^3P + 22 4d8f ^1D + 6 4d7f ^1D
392 544.30	391 525	1019	4	56 4d8f ^1G + 27 4d8f ^3H
393 980.20	394 029	−49	3	67 4d8f ^3G
394 631.20	394 261	370	1	45 $4p^5 4d^2 5s(^3F)^3D$ + 21 4d8f ^3D + 7 $4p^5 4d^2 5s(^3P)^3D$
395 094.50	394 590	504	3	37 4d8f ^3D + 16 $4p^5 4d^3(^4P)^3D$ + 9 $4p^5 4d^3(^4F)^3D$
395 126.40	395 145	−19	2	30 $4p^5 4d^2 5s(^3F)^3D$ + 29 4d8f ^3F
396 426.70	396 630	−206	5	53 4d8f ^3G + 15 4d8f ^1H + 7 4d9f ^3G
397 682.60	397 103	580	3	27 4d8f ^3F + 27 $4p^5 4d^2 5s(^3P)^5P$ + 9 $4p^5 4d^3(^4F)^3F$
398 182.60	397 729	454	2	20 4d8f ^1D + 11 4d8f ^3P
401 055.80	401 385	−329	1	47 4d9f ^3D + 18 $4p^5 4d^3(^4F)^3D$ + 14 4d9f ^1P
401 751.20	401 834	−83	4	46 4d9f ^3H + 45 4d9f ^1G
401 997.40	401 396	601	2	46 4d9f ^3D + 17 $4p^5 4d^3(^4F)^3D$ + 7 4d9f ^3F

Table A.7. Comparison between available experimental and calculated energy levels in Mo VI. Energies are given in cm^{-1}.

E_{exp} [a]	E_{calc} [b]	ΔE	J	Leading components (in %) in LS coupling [c]
				Even parity
0.00	0	0	1.5	99 $4d\ ^2D$
2583.50	2583	0	2.5	99 $4d\ ^2D$
119 725.62	119 725	0	0.5	99 $5s\ ^2S$
282 825.59	282 825	0	1.5	99 $5d\ ^2D$
283 610.94	283 611	0	2.5	99 $5d\ ^2D$
313 806.81	313 807	0	0.5	100 $6s\ ^2S$
386 165.59	386 166	0	1.5	99 $6d\ ^2D$
386 552.16	386 552	0	2.5	99 $6d\ ^2D$
395 181.34	395 181	0	3.5	100 $5g\ ^2G$
395 184.31	395 184	0	4.5	100 $5g\ ^2G$
400 761.59	400 762	0	0.5	100 $7s\ ^2S$
439 465.16	439 465	0	1.5	99 $7d\ ^2D$
439 691.28	439 691	0	2.5	99 $7d\ ^2D$
443 937.56	443 938	0	3.5	100 $6g\ ^2G$
443 941.00	443 941	0	4.5	100 $6g\ ^2G$
447 730.19	447 730	0	0.5	100 $8s\ ^2S$
470 813.00	470 813	0	1.5	99 $8d\ ^2D$
470 962.00	470 962	0	2.5	99 $8d\ ^2D$
473 433.70	473 434	0	3.5	100 $7g\ ^2G$
473 437.06	473 437	0	4.5	100 $7g\ ^2G$
474 431.80	474 432	0	5.5	100 $7i\ ^2I$
474 435.50	474 436	0	6.5	100 $7i\ ^2I$
492 596.81	492 597	0	3.5	100 $8g\ ^2G$
492 601.06	492 601	0	4.5	100 $8g\ ^2G$
493 347.38	493 347	0	5.5	100 $8i\ ^2I$
493 348.19	493 348	0	6.5	100 $8i\ ^2I$
				Odd parity
182 404.47	182 404	0	0.5	99 $5p\ ^2P$
187 331.19	187 331	0	1.5	99 $5p\ ^2P$
267 047.22	266 941	106	2.5	86 $4f\ ^2F$ + 11 $4p^5 4d^2(^1G)^2F$
267 456.84	267 566	−109	3.5	87 $4f\ ^2F$ + 8 $4p^5 4d^2(^1G)^2F$
286 236.00	286 288	−52	0.5	85 $4p^5 4d^2(^3F)^4D$ + 13 $4p^5 4d^2(^3P)^4D$
287 250.00	287 263	−13	1.5	78 $4p^5 4d^2(^3F)^4D$ + 16 $4p^5 4d^2(^3P)^4D$
288 938.00	288 902	36	2.5	67 $4p^5 4d^2(^3F)^4D$ + 22 $4p^5 4d^2(^3P)^4D$ + 6 $4p^5 4d^2(^3F)^4F$
300 690.00	300 600	90	2.5	87 $4p^5 4d^2(^3P)^4P$
303 186.00	303 246	−60	2.5	21 $4p^5 4d^2(^3F)^4F$ + 38 $4p^5 4d^2(^3F)^4G$ + 15 $4p^5 4d^2(^3F)^2F$
304 074.00	304 043	31	1.5	82 $4p^5 4d^2(^3P)^4P$
306 806.00	306 871	−65	1.5	32 $4p^5 4d^2(^1D)^2D$ + 36 $4p^5 4d^2(^3F)^4F$ + 12 $4p^5 4d^2(^3F)^2D$
307 386.00	307 433	−47	0.5	87 $4p^5 4d^2(^3P)^4P$ + 5 $4p^5 4d^2(^3P)^2S$
308 874.00	308 782	92	2.5	54 $4p^5 4d^2(^1D)^2D$ + 15 $4p^5 4d^2(^3F)^2D$ + 9 $4p^5 4d^2(^3F)^4G$
312 090.37	311 918	172	3.5	39 $4p^5 4d^2(^3F)^4F$ + 31 $4p^5 4d^2(^3F)^2G$ + 11 $4p^5 4d^2(^3F)^4G$
314 953.00	314 784	169	1.5	50 $4p^5 4d^2(^3F)^4F$ + 20 $4p^5 4d^2(^1D)^2P$ + 11 $4p^5 4d^2(^1D)^2D$
315 155.49	315 212	−57	2.5	21 $4p^5 4d^2(^1G)^2F$ + 31 $4p^5 4d^2(^3F)^4F$ + 17 $4p^5 4d^2(^3F)^2F$
315 795.00	316 117	−322	0.5	68 $4p^5 4d^2(^1D)^2P$ + 19 $4p^5 4d^2(^3P)^2P$ + 6 $4p^5 4d^2(^3P)^4P$
316 476.56	316 845	−368	3.5	25 $4p^5 4d^2(^3F)^2F$ + 25 $4p^5 4d^2(^1G)^2F$ + 23 $4p^5 4d^2(^3P)^4D$
318 528.00	318 313	215	2.5	47 $4p^5 4d^2(^3F)^4G$ + 28 $4p^5 4d^2(^3F)^4F$ + 11 $4p^5 4d^2(^1G)^2F$
320 088.00	319 864	224	3.5	90 $4p^5 4d^2(^1D)^2F$ + 5 $4f\ ^2F$
329 873.00	329 987	−114	2.5	50 $4p^5 4d^2(^3P)^4D$ + 26 $4p^5 4d^2(^3F)^4D$ + 14 $4p^5 4d^2(^3P)^2D$
331 208.00	331 187	21	3.5	41 $4p^5 4d^2(^3P)^4D$ + 39 $4p^5 4d^2(^3F)^4D$ + 8 $4p^5 4d^2(^3F)^4F$
331 693.00	331 458	235	1.5	47 $4p^5 4d^2(^3P)^4D$ + 29 $4p^5 4d^2(^3P)^2D$ + 12 $4p^5 4d^2(^3F)^4D$
337 018.00	336 961	57	0.5	82 $4p^5 4d^2(^3P)^4D$ + 12 $4p^5 4d^2(^3F)^4D$
337 071.03	337 150	−79	2.5	81 $4p^5 4d^2(^1D)^2F$
340 570.78	340 571	0	0.5	99 $6p\ ^2P$
342 562.44	342 544	18	1.5	88 $6p\ ^2P$ + 5 $4p^5 4d^2(^3P)^2D$
343 114.50	343 261	−146	1.5	45 $4p^5 4d^2(^3P)^2D$ + 24 $4p^5 4d^2(^3P)^4D$ + 11 $6p\ ^2P$
346 888.80	346 902	−13	1.5	77 $4p^5 4d^2(^3P)^4S$ + 6 $4p^5 4d^2(^3P)^2D$ + 5 $4p^5 4d^2(^3P)^4P$
348 702.28	348 602	100	3.5	84 $4p^5 4d^2(^1G)^2G$ + 9 $4p^5 4d^2(^3F)^2F$
349 283.97	349 427	−143	2.5	65 $4p^5 4d^2(^3P)^2D$ + 14 $4p^5 4d^2(^3P)^4D$ + 6 $4p^5 4d^2(^3F)^2D$
355 442.00	355 442	0	1.5	69 $4p^5 4d^2(^1S)^2P$ + 26 $4p^5 4d^2(^1D)^2P$
365 103.41	365 240	−137	2.5	51 $5f\ ^2F$ + 26 $4p^5 4d^2(^3F)^2F$ + 14 $4p^5 4d^2(^1G)^2F$

Notes. [a] From Reader (2010). [b] This work. [c] Only the first three components that are larger than 5% are given.

Table A.7. conitnued.

E_{exp} [a]	E_{calc} [b]	ΔE	J	Leading components (in %) in LS coupling[c]
368 203.16	368 087	116	3.5	65 5f ^{2}F + 16 4p^{5}4d^2(^{3}F)^{2}F + 11 4p^{5}4d^2(^{1}G)^{2}F
394 045.41	394 049	−4	2.5	23 4p^{5}4d^2(^{3}F)^{2}F + 45 5f ^{2}F + 21 4p^{5}4d^2(^{1}G)^{2}F
398 931.69	398 943	−11	3.5	28 4p^{5}4d^2(^{1}G)^{2}F + 33 5f ^{2}F + 25 4p^{5}4d^2(^{3}F)^{2}F
403 120.00	403 201	−81	0.5	68 4p^{5}4d^2(^{3}P)^{2}P + 16 4p^{5}4d^2(^{1}S)^{2}P + 11 4p^{5}4d^2(^{1}D)^{2}P
407 906.00	407 574	332	1.5	71 4p^{5}4d^2(^{3}P)^{2}P + 16 4p^{5}4d^2(^{1}D)^{2}P + 6 4p^{5}4d^2(^{1}S)^{2}P
412 799.00	412 832	−33	2.5	68 4p^{5}4d^2(^{3}F)^{2}D + 15 4p^{5}4d^2(^{1}D)^{2}D + 11 4p^{5}4d^2(^{3}P)^{2}D
413 282.00	413 433	−151	1.5	70 4p^{5}4d^2(^{3}F)^{2}D + 17 4p^{5}4d^2(^{1}D)^{2}D + 9 4p^{5}4d^2(^{3}P)^{2}D
414 853.81	414 849	5	0.5	95 7p ^{2}P
416 068.59	416 079	−10	1.5	95 7p ^{2}P
417 695.00	417 842	−147	0.5	97 4p^{5}4d5s(^{3}P)^{4}P
420 665.00	420 788	−123	1.5	93 4p^{5}4d5s(^{3}P)^{4}P
426 499.00	426 529	−30	2.5	88 4p^{5}4d5s(^{3}P)^{4}P + 8 4p^{5}4d5s(^{3}D)^{4}D
427 009.00	427 117	−108	0.5	91 4p^{5}4d5s(^{3}P)^{2}P
431 560.00	431 267	293	3.5	87 4p^{5}4d5s(^{3}F)^{4}F
433 184.00	433 248	−64	1.5	82 4p^{5}4d5s(^{3}P)^{2}P + 6 4p^{5}4d5s(^{3}D)^{2}D + 5 4p^{5}4d5s(^{3}D)^{4}D
434 125.00	433 861	264	2.5	74 4p^{5}4d5s(^{3}F)^{4}F + 8 4p^{5}4d5s(^{1}F)^{2}F + 8 4p^{5}4d5s(^{3}F)^{2}F
436 181.50	436 073	109	2.5	93 6f ^{2}F
436 548.31	436 660	−112	3.5	90 6f ^{2}F
437 890.00	437 793	97	1.5	69 4p^{5}4d5s(^{3}F)^{4}F + 19 4p^{5}4d5s(^{1}D)^{2}D + 7 4p^{5}4d5s(^{3}D)^{4}D
437 978.00	437 737	241	3.5	89 4p^{5}4d5s(^{3}F)^{2}F + 6 4p^{5}4d5s(^{3}D)^{4}D
441 562.00	441 598	−36	2.5	54 4p^{5}4d5s(^{3}F)^{2}F + 22 4p^{5}4d5s(^{1}D)^{2}D + 13 4p^{5}4d5s(^{3}D)^{4}D
445 102.50	445 103	0	4.5	100 6h ^{2}H
445 106.20	445 106	0	5.5	100 6h ^{2}H
448 052.00	448 205	−153	3.5	68 4p^{5}4d5s(^{3}D)^{4}D + 30 4p^{5}4d5s(^{1}F)^{2}F
451 836.00	451 995	−159	2.5	38 4p^{5}4d5s(^{3}D)^{2}D + 32 4p^{5}4d5s(^{1}F)^{2}F + 24 4p^{5}4d5s(^{3}D)^{4}D
454 862.00	454 942	−80	0.5	72 4p^{5}4d5s(^{3}D)^{4}D + 24 8p ^{2}P
455 807.00	455 769	38	1.5	57 4p^{5}4d5s(^{3}D)^{4}D + 18 4p^{5}4d5s(^{3}F)^{4}F + 12 4p^{5}4d5s(^{1}D)^{2}D
456 494.90	456 469	26	0.5	75 8p ^{2}P + 22 4p^{5}4d5s(^{3}D)^{4}D
456 718.34	456 722	−4	1.5	86 8p ^{2}P + 7 4p^{5}4d5s(^{1}D)^{2}D
458 214.00	458 360	−146	2.5	33 4p^{5}4d5s(^{1}D)^{2}D + 19 4p^{5}4d5s(^{3}F)^{2}F + 18 4p^{5}4d5s(^{3}F)^{4}F
458 942.00	458 974	−32	1.5	42 4p^{5}4d5s(^{1}D)^{2}D + 24 4p^{5}4d5s(^{3}D)^{2}D + 19 4p^{5}4d5s(^{3}D)^{4}D
462 578.00	462 592	−14	2.5	34 4p^{5}4d5s(^{3}D)^{4}D + 39 4p^{5}4d5s(^{1}D)^{2}D + 11 4p^{5}4d5s(^{3}D)^{2}D
466 403.00	466 383	20	1.5	65 4p^{5}4d5s(^{3}D)^{2}D + 17 4p^{5}4d5s(^{1}D)^{2}D + 11 4p^{5}4d5s(^{3}P)^{2}P
466 410.00	466 382	28	3.5	61 4p^{5}4d5s(^{1}F)^{2}F + 22 4p^{5}4d5s(^{3}D)^{4}D + 11 4p^{5}4d5s(^{3}F)^{4}F
467 829.78	467 813	16	2.5	98 7f ^{2}F
467 944.41	467 961	−17	3.5	98 7f ^{2}F
469 446.00	469 357	89	2.5	42 4p^{5}4d5s(^{1}F)^{2}F + 39 4p^{5}4d5s(^{3}D)^{2}D + 14 4p^{5}4d5s(^{3}F)^{2}F
474 295.97	474 295	1	4.5	100 7h ^{2}H
474 296.78	474 297	0	5.5	100 7h ^{2}H
481 343.00	481 343	0	0.5	100 9p ^{2}P
481 768.00	481 768	0	1.5	100 9p ^{2}P
488 713.00	488 701	12	2.5	99 8f ^{2}F
488 752.00	488 764	−12	3.5	99 8f ^{2}F
493 245.00	493 246	−1	4.5	100 8h ^{2}H
493 248.34	493 247	1	5.5	100 8h ^{2}H
493 377.60	493 378	0	6.5	100 8k ^{2}K
493 381.30	493 378	3	7.5	100 8k ^{2}K
498 038.00	498 038	0	0.5	100 10p ^{2}P
498 300.00	498 300	0	1.5	100 10p ^{2}P
502 976.00	502 977	−1	2.5	100 9f ^{2}F
503 014.00	503 013	1	3.5	100 9f ^{2}F
509 596.00	509 596	0	0.5	100 11p ^{2}P
509 786.00	509 786	0	1.5	100 11p ^{2}P

Table A.8. Comparison between available experimental and calculated energy levels in Mo VII. Energies are given in cm^{-1}.

E_{exp} [a]	E_{calc} [b]	ΔE	J	Leading components (in %) in LS coupling[c]
				Even parity
0.00	0	0	0	97 $4p^6\ ^1S$
542 265.29	542 456	−191	1	80 $4p^5 5p\ ^3S$ + 17 $4p^5 5p\ ^3P$
544 663.10	544 655	8	1	73 $4s4p^6 4d\ ^3D$ + 12 $4p^4(^1D)4d^2\ ^3D$ + 8 $4p^5 4f\ ^3D$
545 906.83	545 883	24	2	73 $4s4p^6 4d\ ^3D$ + 11 $4p^4(^1D)4d^2\ ^3D$ + 8 $4p^5 4f\ ^3D$
548 077.57	547 987	91	2	55 $4p^5 5p\ ^3D$ + 35 $4p^5 5p\ ^1D$ + 8 $4p^5 5p\ ^3P$
548 120.43	548 120	0	3	74 $4s4p^6 4d\ ^3D$ + 12 $4p^4(^1D)4d^2\ ^3D$ + 7 $4p^5 4f\ ^3D$
552 329.97	552 000	330	3	98 $4p^5 5p\ ^3D$
554 401.01	554 408	−7	1	48 $4p^5 5p\ ^1P$ + 28 $4p^5 5p\ ^3D$ + 18 $4p^5 5p\ ^3P$
557 437.49	557 605	−168	2	65 $4p^5 5p\ ^3P$ + 29 $4p^5 5p\ ^1D$
563 567.72	563 589	−21	2	62 $4s4p^6 4d\ ^1D$ + 18 $4p^4(^1D)4d^2\ ^1D$ + 9 $4p^4(^1D)4d^2\ ^1D$
565 803.85	565 892	−88	0	77 $4p^5 5p\ ^3P$ + 22 $4p^5 5p\ ^1S$
570 658.75	570 618	41	1	64 $4p^5 5p\ ^3D$ + 33 $4p^5 5p\ ^1P$
577 644.10	577 596	48	2	34 $4p^5 5p\ ^1D$ + 41 $4p^5 5p\ ^3D$ + 23 $4p^5 5p\ ^3P$
577 765.90	577 851	−85	1	63 $4p^5 5p\ ^3P$ + 18 $4p^5 5p\ ^1P$ + 13 $4p^5 5p\ ^3S$
585 026.11	585 000	26	0	76 $4p^5 5p\ ^1S$ + 23 $4p^5 5p\ ^3P$
609 898.90	606 995	2904	2	42 $4p^4(^3P)4d^2\ ^5D$ + 22 $4p^4(^3P)4d^2\ ^5F$ + 15 $4p^4(^3P)4d^2\ ^5D$
610 564.98	610 483	82	5	70 $4p^5 4f\ ^3G$ + 24 $4p^4(^3P)4d^2\ ^3G$
610 908.23	610 998	−90	4	47 $4p^5 4f\ ^3G$ + 22 $4p^5 4f\ ^1G$ + 19 $4p^4(^3P)4d^2\ ^3G$
611 395.80	614 262	−2866	4	40 $4p^4(^3P)4d^2\ ^5F$ + 29 $4p^4(^3P)4d^2\ ^5D$ + 11 $4p^4(^3P)4d^2\ ^5G$
611 727.25	611 765	−38	1	54 $4p^5 4f\ ^3D$ + 13 $4p^4(^3P)4d^2\ ^5F$ + 10 $4p^4(^3P)4d^2\ ^3D$
613 593.09	613 685	−92	2	43 $4p^5 4f\ ^3D$ + 8 $4p^5 4f\ ^3F$ + 7 $4p^4(^3P)4d^2\ ^3D$
615 203.92	615 179	25	3	24 $4p^5 4f\ ^3F$ + 24 $4p^5 4f\ ^3G$ + 11 $4p^4(^3P)4d^2\ ^3G$
615 725.35	615 720	5	3	22 $4p^4(^3P)4d^2\ ^5F$ + 17 $4p^4(^3P)4d^2\ ^5D$ + 16 $4p^5 4f\ ^3D$
616 148.25	616 162	−14	4	38 $4p^5 4f\ ^3F$ + 21 $4p^4(^3P)4d^2\ ^3F$ + 20 $4p^5 4f\ ^1G$
624 603.86	624 455	149	2	26 $4p^5 4f\ ^3F$ + 16 $4p^5 4f\ ^1D$ + 12 $4p^5 4f\ ^3D$
633 788.90	633 559	230	3	24 $4p^5 4f\ ^3G$ + 19 $4p^5 4f\ ^3F$ + 18 $4p^4(^3P)4d^2\ ^3G$
635 262.40	635 075	187	4	32 $4p^5 4f\ ^1G$ + 18 $4p^4(^3P)4d^2\ ^3F$ + 11 $4p^5 4f\ ^3G$
635 910.50	636 296	−385	3	30 $4p^5 4f\ ^1F$ + 19 $4p^5 4f\ ^3D$ + 6 $4p^4(^3P)4d^2\ ^3F$
645 811.86	645 895	−83	2	26 $4p^5 4f\ ^1D$ + 11 $4p^4(^1D)4d^2\ ^1D$ + 8 $4p^5 4f\ ^3F$
648 282.60	647 870	413	4	43 $4p^4(^3P)4d^2\ ^5D$ + 24 $4p^4(^3P)4d^2\ ^5D$ + 6 $4p^4(^3P)4d^2\ ^3F$
771 708.20	770 648	1060	1	15 $4p^4(^3P)4d^2\ ^3P$ + 29 $4p^5 5f\ ^3D$ + 11 $4p^4(^1S)4d^2\ ^3P$
773 033.30	769 815	3218	2	56 $4p^5 5f\ ^3D$ + 13 $4p^5 5f\ ^3F$ + 8 $4p^4(^3P)4d^2\ ^3D$
774 110.00	774 662	−552	5	88 $4p^5 5f\ ^3G$ + 7 $4p^4(^3P)4d^2\ ^3G$
775 406.00	775 927	−521	4	65 $4p^5 5f\ ^3G$ + 12 $4p^5 5f\ ^1G$ + 11 $4p^5 5f\ ^3F$
775 781.00	774 531	1250	3	45 $4p^5 5f\ ^3D$ + 15 $4p^5 5f\ ^3F$ + 15 $4p^4(^3P)4d^2\ ^1F$
776 649.60	778 934	−2284	2	20 $4p^4(^1D)4d^2\ ^3D$ + 21 $4p^5 5f\ ^3D$ + 16 $4p^4(^3P)4d^2\ ^3D$
777 161.10	777 843	−682	3	33 $4p^5 5f\ ^3G$ + 32 $4p^5 5f\ ^1F$ + 22 $4p^5 5f\ ^3F$
779 373.60	781 310	−1936	4	48 $4p^5 5f\ ^3F$ + 30 $4p^5 5f\ ^1G$
794 751.20	794 987	−236	2	59 $4p^5 5f\ ^3F$ + 13 $4p^5 5f\ ^1D$ + 13 $4p^5 5f\ ^3D$
797 800.50	797 278	522	3	43 $4p^5 5f\ ^1F$ + 35 $4p^5 5f\ ^3G$ + 13 $4p^5 5f\ ^3D$
797 995.40	797 598	397	3	45 $4p^5 5f\ ^3F$ + 23 $4p^5 5f\ ^3G$ + 18 $4p^5 5f\ ^3D$
800 199.70	800 881	−681	4	33 $4p^5 5f\ ^1G$ + 25 $4p^5 5f\ ^3G$ + 22 $4p^5 5f\ ^3F$
				Odd parity
302 343.70	302 618	−274	0	99 $4p^5 4d\ ^3P$
305 558.90	305 795	−236	1	96 $4p^5 4d\ ^3P$
312 048.40	312 226	−178	2	88 $4p^5 4d\ ^3P$ + 9 $4p^5 4d\ ^3D$
315 491.80	314 944	548	4	99 $4p^5 4d\ ^3F$
318 103.90	317 625	479	3	83 $4p^5 4d\ ^3F$ + 10 $4p^5 4d\ ^1F$ + 6 $4p^5 4d\ ^3D$
322 896.00	322 759	137	2	66 $4p^5 4d\ ^3F$ + 20 $4p^5 4d\ ^1D$ + 13 $4p^5 4d\ ^3D$
333 618.90	334 040	−421	3	64 $4p^5 4d\ ^3D$ + 35 $4p^5 4d\ ^1F$
341 503.80	341 537	−33	2	45 $4p^5 4d\ ^1D$ + 33 $4p^5 4d\ ^3F$ + 21 $4p^5 4d\ ^3D$
341 713.00	341 727	−14	1	95 $4p^5 4d\ ^3D$
347 433.40	347 624	−191	2	57 $4p^5 4d\ ^3D$ + 31 $4p^5 4d\ ^1D$ + 11 $4p^5 4d\ ^3P$
351 126.60	350 945	182	3	55 $4p^5 4d\ ^1F$ + 29 $4p^5 4d\ ^3D$ + 16 $4p^5 4d\ ^3F$
417 528.60	417 528	1	1	96 $4p^5 4d\ ^1P$
477 767.80	477 772	−4	2	99 $4p^5 5s\ ^3P$
481 295.99	481 291	5	1	53 $4p^5 5s\ ^1P$ + 45 $4p^5 5s\ ^3P$
500 618.75	500 613	6	0	99 $4p^5 5s\ ^3P$
502 933.27	502 939	−6	1	53 $4p^5 5s\ ^3P$ + 45 $4p^5 5s\ ^1P$

Notes. [a] From Reader (2010). [b] This work. [c] Only the first three components that are larger than 5% are given.

Table A.8. continued.

E_{exp} [a]	E_{calc} [b]	ΔE	J	Leading components (in %) in LS coupling[c]
657 602.91	657 637	−34	0	99 $4p^5 5d\ ^3P$
659 015.62	659 037	−21	1	88 $4p^5 5d\ ^3P$ + 9 $4p^5 5d\ ^3D$
661 488.47	661 358	130	4	99 $4p^5 5d\ ^3F$
661 678.46	661 689	−11	2	64 $4p^5 5d\ ^3P$ + 26 $4p^5 5d\ ^3D$ + 8 $4p^5 5d\ ^1D$
661 683.19	661 680	3	3	58 $4p^5 5d\ ^3F$ + 38 $4p^5 5d\ ^1F$
664 362.66	664 363	0	2	46 $4p^5 5d\ ^1D$ + 31 $4p^5 5d\ ^3F$ + 21 $4p^5 5d\ ^3D$
665 713.78	665 693	21	3	67 $4p^5 5d\ ^3D$ + 27 $4p^5 5d\ ^1F$
669 063.09	669 155	−92	1	46 $4p^5 5d\ ^3D$ + 50 $4p^5 5d\ ^1P$
684 805.34	684 824	−19	2	66 $4p^5 5d\ ^3F$ + 25 $4p^5 5d\ ^1D$ + 7 $4p^5 5d\ ^3D$
686 113.49	686 168	−55	2	45 $4p^5 5d\ ^3D$ + 32 $4p^5 5d\ ^3P$ + 20 $4p^5 5d\ ^1D$
686 635.00	686 656	−21	3	34 $4p^5 5d\ ^1F$ + 37 $4p^5 5d\ ^3F$ + 29 $4p^5 5d\ ^3D$
689 784.69	689 687	98	1	47 $4p^5 5d\ ^1P$ + 43 $4p^5 5d\ ^3D$ + 8 $4p^5 5d\ ^3P$
708 843.60	708 839	5	2	100 $4p^5 6s\ ^3P$
710 068.90	710 073	−5	1	62 $4p^5 6s\ ^1P$ + 37 $4p^5 6s\ ^3P$
731 864.90	731 872	−7	0	99 $4p^5 6s\ ^3P$
732 582.50	732 575	8	1	62 $4p^5 6s\ ^3P$ + 37 $4p^5 6s\ ^1P$
780 390.00	780 389	1	1	60 $4s4p^6 5p\ ^3P$ + 18 $4p^4(^1D)4d5p\ ^3P$ + 13 $4p^5 6d\ ^3P$
789 696.00	789 687	9	1	61 $4s4p^6 5p\ ^1P$ + 20 $4p^4(^1D)4d5p\ ^1P$ + 8 $4p^5 6d\ ^3P$
793 700.50	793 689	11	2	75 $4p^5 5g\ ^3F$ + 12 $4p^5 6d\ ^3D$
793 909.10	794 182	−273	3	42 $4p^5 5g\ ^3F$ + 31 $4p^5 6d\ ^3D$ + 13 $4p^5 5g\ ^1F$
794 550.20	794 567	−17	6	99 $4p^5 5g\ ^3H$
794 669.80	794 661	9	5	52 $4p^5 5g\ ^1H$ + 47 $4p^5 5g\ ^3H$
795 532.00	795 626	−94	1	54 $4p^5 6d\ ^1P$ + 37 $4p^5 6d\ ^3D$ + 6 $4s4p^6 5p\ ^1P$
795 665.20	795 574	91	4	49 $4p^5 5g\ ^3F$ + 28 $4p^5 5g\ ^3G$ + 22 $4p^5 5g\ ^1G$
795 918.60	795 923	−4	3	39 $4p^5 5g\ ^1F$ + 49 $4p^5 5g\ ^3G$ + 9 $4p^5 5g\ ^3F$
796 389.50	796 411	−21	4	38 $4p^5 5g\ ^1G$ + 31 $4p^5 5g\ ^3H$ + 30 $4p^5 5g\ ^3G$
796 442.60	796 470	−27	5	68 $4p^5 5g\ ^3G$ + 16 $4p^5 5g\ ^1H$ + 15 $4p^5 5g\ ^3H$
816 413.00	817 148	−735	1	61 $4p^5 7s\ ^1P$ + 33 $4p^5 7s\ ^3P$
818 278.10	818 257	21	4	26 $4p^5 5g\ ^3G$ + 49 $4p^5 5g\ ^3F$ + 23 $4p^5 5g\ ^1G$
818 504.10	818 503	1	4	68 $4p^5 5g\ ^3H$ + 16 $4p^5 5g\ ^1G$ + 15 $4p^5 5g\ ^3G$
818 583.40	818 606	−23	3	48 $4p^5 5g\ ^3G$ + 30 $4p^5 5g\ ^1F$ + 20 $4p^5 5g\ ^3F$
818 597.80	818 598	0	5	37 $4p^5 5g\ ^3H$ + 31 $4p^5 5g\ ^1H$ + 31 $4p^5 5g\ ^3G$
839 342.00	839 304	38	1	65 $4p^5 7s\ ^3P$ + 35 $4p^5 7s\ ^1P$
874 998.00	874 906	92	1	43 $4p^5 8s\ ^1P$ + 22 $4p^5 8s\ ^3P$ + 9 $4p^4(^1D)4d5p\ ^3D$
898 093.00	897 197	896	1	38 $4p^5 8s\ ^3P$ + 19 $4p^5 8s\ ^1P$ + 6 $4p^4(^3P)4d5p\ ^3P$
910 830.00	910 688	142	1	63 $4p^5 9s\ ^1P$ + 33 $4p^5 9s\ ^3P$
934 536.00	934 473	63	1	65 $4p^5 10s\ ^1P$ + 33 $4p^5 10s\ ^3P$

Table A.9. Comparison of wavelengths and log gf values of the identified Mo V and Mo VI lines to literature values.

Ion	Transition	Energy/cm^{-1}		λ/Å	log gf	λ/Å	log gf
		lower level	upper level	this work		literature	
Mo V	5p ^{3}P$^\circ_{2.0}$–6s ^{5}5/2[5/2]$_{3.0}$	157 851	256 676	1011.889	−0.12	1011.891	−0.16[a]
	5p ^{1}D$^\circ_{2.0}$–5d ^{3}F$_{2.0}$	146 977	237 760	1101.530	0.01	1101.529	0.07[a]
	5p ^{3}D$^\circ_{1.0}$–5d ^{3}F$_{2.0}$	148 949	237 760	1125.988	0.22	1125.990	0.31[a]
	5p $^3F^\circ_{3.0}$–5d ^{3}F$_{3.0}$	151 195	239 069	1137.995	0.32	1137.999	0.39[a]
	5p ^{3}D$^\circ_{3.0}$–5d ^{3}F$_{4.0}$	153 040	240 110	1148.502	0.45	1148.504	0.52[a]
	5p $^3F^\circ_{3.0}$–5d ^{3}G$_{4.0}$	151 195	235 496	1186.227	0.52	1186.230	0.57[a]
	5p ^{3}D$^\circ_{1.0}$–5d ^{3}D$_{1.0}$	148 949	233 190	1187.061	0.03	1187.061	0.10[a]
	5s ^{3}D$_{3.0}$–5p ^{3}P$^\circ_{2.0}$	94 835	157 851	1586.898	0.01	1586.890	0.09[a]
	5s ^{1}D$_{2.0}$–5p ^{1}P$^\circ_{1.0}$	99 380	162 257	1590.414	−0.08	1590.415	0.01[a]
	5s ^{1}D$_{2.0}$–5p $^1F^\circ_{3.0}$	99 380	159 857	1653.541	0.28	1653.541	0.35[a]
	5s ^{3}D$_{3.0}$–5p $^3F^\circ_{4.0}$	94 835	155 032	1661.215	0.44	1661.215	0.51[a]
	5s ^{3}D$_{2.0}$–5p ^{3}D$^\circ_{3.0}$	93 111	153 040	1668.662	0.15	1668.660	0.24[a]
Mo VI	5p ^{2}P$^\circ_{1/2}$–5d ^{2}D$_{3/2}$	182 404	282 826	995.806	0.35	995.811	0.44[b]
	5p ^{2}P$^\circ_{3/2}$–5d ^{2}D$_{5/2}$	187 331	283 611	1038.640	0.59	1038.642	0.67[b]
	5p ^{2}P$^\circ_{3/2}$–5d ^{2}D$_{3/2}$	187 331	282 826	1047.182	−0.37	1047.184	−0.28[b]
	5d ^{2}D$_{5/2}$–5f $^2F^\circ_{7/2}$	283 611	368 203	1182.142	0.65	1182.143	0.72[b]
	5g ^{2}G$_{9/2}$–7h ^{2}H$^\circ_{11/2}$	395 184	474 297	1264.023	0.31	1264.052	0.32[b,c]
	4d^2 $^2F^\circ_{7/2}$–5g ^{2}G$_{7/2}$	316 477	395 184	1270.523	−1.04	1270.520	−0.91[b]
	4d^2 $^2F^\circ_{7/2}$–6d ^{2}D$_{5/2}$	316 477	386 552	1427.030	−2.22	–	–
	5s ^{2}S$_{1/2}$–5p ^{2}P$^\circ_{3/2}$	119 726	187 331	1479.168	0.09	1479.168	0.15[b]
	5s $^2S_{1/2}$–5p ^{2}P$^\circ_{1/2}$	119 726	182 404	1595.435	−0.25	1595.435	−0.18[b]

Notes. [(a)] Reader & Tauheed (2015); [(b)] Reader (2010), Mo VI λ 1427.030 Å is not listed; [(c)] blend with 5g ^{2}G$_{7/2}$–7h ^{2}H$^\circ_{9/2}$, λ 1264.017 Å, log gf = 0.23.